International Journal of Pharmaceutics 636 (2023) 122866

Contents lists available at ScienceDirect

International Journal of Pharmaceutics

journal homepage: www.elsevier.com/locate/ijpharm

Reprogramming of tumor-associated macrophages by polyaniline-coated iron oxide nanoparticles applied to treatment of breast cancer

Camila Nascimento [a], Flávia Castro [b,c,1], Mariana Domingues [b,c,d,1], Anna Lage [a], Érica Alves [a], Rodrigo de Oliveira [a], Celso de Melo [e], Carlos Eduardo Calzavara-Silva [a], Bruno Sarmento [b,c,f,*,1]

[a] Grupo de Pesquisa em Imunologia Celular e Molecular, Instituto René Rachou - Fiocruz Minas, Av. Augusto de Lima, 1715 - Barro Preto, Belo Horizonte, MG 30190-002, Brazil
[b] INEB - Instituto Nacional de Engenharia Biomédica, Universidade do Porto, Rua Alfredo Allen, 208, 4200-135 Porto, Portugal
[c] i3S - Instituto de Investigação e Inovação em Saúde, Universidade do Porto, Rua Alfredo Allen 208, 4200-135 Porto, Portugal
[d] FEUP - Faculdade de Engenharia da Universidade do Porto, Rua Doutor Roberto Frias, 4200-465 Porto, Portugal
[e] Grupo de Polímeros Não-Convencionais, Departamento de Física, Universidade Federal de Pernambuco, Av. Prof. Moraes Rego, 1235 - Cidade Universitária, Recife, PE 50670-901, Brazil
[f] CESPU - IUCS, Rua Central da Gandra, 137, 4585-116 Gandra, Portugal

ARTICLE INFO

Keywords:
Breast cancer
Iron oxide nanoparticles
Immunomodulation
Macrophages
Tumor microenvironment
3D models

ABSTRACT

Breast cancer is the most commonly diagnosed type of cancer among the female population worldwide. It is a disease with a high incidence and geographic distribution that negatively impacts global public health and deleteriously affect the quality of life of cancer patients. Among the new approaches, cancer immunotherapy is the most promising trend in oncology by stimulating the host's own immune system to efficiently destroy cancer cells. Recent evidence has indicated that iron oxide nanoparticles can promote the reprograming of M2 into M1 macrophages with anti-tumor effects in the tumor microenvironment. Thus, the aim of the present work was to evaluate the ability of polyaniline-coated maghemite (Pani/γ-Fe_2O_3) nanoparticles to modulate human macrophages in 2D monolayers and 3D multicellular breast cancer models. It was observed that Pani/γ-Fe_2O_3 NPs re-educated IL-10-stimulated macrophages towards a pro-inflammatory profile, decreasing the proportion of $CD163^+$ and increasing the $CD86^+$ proportion in 2D models. NPs were successfully taken-up by macrophages presented in the 3D model and were also able to induce an increasing in their $CD86^+$ proportion in triple MCTs model. Overall, our findings open new perspectives on the use of Pani/γ-Fe_2O_3 NPs as an immunomodulatory therapy for macrophage reprogramming towards an anti-tumor M1 phenotype, providing a new tool for breast cancer immunotherapies.

1. Introduction

Breast cancer is the most diagnosed cancer among woman population worldwide. It is a disease with a high incidence and geographic distribution, which has a negative impact on global public health by causing physical, socioeconomic and psychological issues, as well as negatively interfering in patients' quality of life (Wild et al., 2020). In 2021, breast cancer has overtaken lung cancer as the world's mostly commonly-diagnosed cancer, according to the International Agency for Research on Cancer (IARC) (Ferlay et al., 2021; Gao and Swain, 2018). Thus, new initiatives and strategies focused on the prevention and treatment of breast cancer must be established to reduce related deaths, promoting breast health and ensuring access to quality care.

Although conventional treatments are very successful in destroying tumor cells, they often destroy healthy cells causing a severe decrease in patient's quality of life (Lukianova-Hleb et al., 2016). In addition, current radio- and chemotherapies are not able to eliminate the critical cancer stem cells, which are protected by specific resistance mechanisms, causing new tumors and metastases more malignant, with fast spreading and resistant to radiotherapy and previously used drugs (Vinogradov and Wei, 2012). The tumor microenvironment (TME) is increasingly recognized as a key player in tumor progression and as a

* Corresponding author at: Nanomedicine and Translational Drug Delivery Group Leader, i3S- Instituto de Investigação e Inovação em Saúde, Universidade do Porto, Rua Alfredo Allen, 208, 4200-135 Porto, Portugal.
E-mail address: bruno.sarmento@i3s.up.pt (B. Sarmento).
[1] Equally contributing second authors.

https://doi.org/10.1016/j.ijpharm.2023.122866
Received 29 November 2022; Received in revised form 3 February 2023; Accepted 14 March 2023
Available online 18 March 2023

promising therapeutic target in breast cancer. There is increasing research in exploring and manipulating the leukocytes of the TME for breast cancer treatment by immunotherapy (Emens, 2018). This alternative treatment is focused on modulating the patient's immune system to identify and fight against cancer. In particular, macrophages, also called tumor-associated macrophages (TAMs), have aroused great interest in recent years as a therapeutic target because they represent a large part of the cellular component of the TME and they can orchestrate an immunosuppressive and pro-tumor microenvironment (Linde et al., 2018).

Macrophages are highly functional plastic cells that constantly change their phenotypic from M2 to M1 in response to tumor environmental stimuli. In the TME, macrophage polarization is regulated by multiple cytokines, chemokines, growth factors and other signals derived from tumor and stromal cells (Murray, 2017). M1 macrophages stimulate the development of the T-helper type 1 (Th1) response and produce TNF-α, IL-1β, IL-12, which are pro-inflammatory cytokines, in addition to reactive oxygen species (ROS) and nitrogen (RNS) (Curren Smith, 2015). Such molecules produced by M1 macrophages are highly toxic and are crucial for host defense and for the destruction of tumor cells (Mantovani et al., 2017). M2 macrophages are induced by IL-4 and IL-13 and stimulate the development of Th2 response with high production of IL-10, TGF-β, chemokines contributing for the immunosuppressive microenvironment maintenance. They are identified by their signature expression of arginase-1, mannose (MMR, CD206), and scavenger receptors (Biswas and Mantovani, 2012; Mantovani et al., 2004). M2 macrophages contribute to attenuating inflammation and promote wound healing, angiogenesis, tissue remodeling and tumor progression (Biswas and Mantovani, 2010).

Due to macrophage plasticity, targeting M2 macrophages to repolarize in the M1 phenotype can be a promising cancer immunotherapy (Furgiuele et al., 2022). Cancer immunotherapy based on the use of iron oxide nanoparticles (IONPs) for macrophage reprogramming is a new strategy that stimulates the host's immune system to destroy cancer cells (Lee Ventola, 2017). Macrophages play an essential role in iron homeostasis and immune defense (Vinchi, 2018). Studies have shown that more than 60% of genes related to iron metabolism, including the differential expression of iron uptake, storage and release, occur between the two final stages of macrophage polarization (Recalcati et al., 2010). M1 macrophages have high levels of the protein ferritin (iron storage) and low levels of the protein ferroportin (iron export) and heme oxygenase-1 (HO-1), which favors a phenotype of intracellular iron sequestration and storage. This leads to enhance of the M1-like effector functions, such as increased pro-inflammatory expression of TNF-α and suppression of the expression of the anti-inflammatory cytokine, IL-10 (Cronin et al., 2019; Fritsche et al., 2008; Jung et al., 2019; Mulero et al., 2002). M2 macrophages exhibit the iron export phenotype, with increased of CD163 and heme oxygenase-1 expression, as well as high levels ferroportin expression and decreased ferritin expression (Recalcati et al., 2019). In the context of the TME, M2-like TAMs are "iron releasers" and support tumor growth and establishment, while M1-like are "iron retainers", being responsible for limiting tumor progression (Jung et al., 2019). Then, the alteration of macrophage phenotype through iron metabolism becomes a suitable tool for cancer treatment (Cronin et al., 2019; Jung et al., 2017).

Studies have shown that IONPs can act directly on the activation of TAMs, leading to the destruction of tumor cells and/or as vehicles for immunomodulatory agents, driving the modulation of the TME and increasing antitumor activity. In 2013, Laskar and collaborators (Laskar et al., 2013) showed that IONPs can induce a phenotypic shift in M2 macrophages to a subtype of M1 macrophages (Laskar et al., 2013). In 2016, Zanganeh and collaborators (Zanganeh et al., 2016), demonstrated that treatment with magnetite nanoparticles encapsulated with carboxymethyl dextran inhibited the growth of breast cancer cells (Zanganeh et al., 2016). The antitumor effect was attributed to the fact that IONPs induced macrophage polarization to M1 phenotype, which produced high levels of TNF-α and ROS (Zanganeh et al., 2016). In another study, Da Silva *et al.* (Costa da Silva et al., 2017) showed through *in vitro* and *in vivo* experiments that TAMs exposed to cross-linked iron oxide (CLIO)-FITC nanoparticles were converted into pro-inflammatory macrophages able of destroying cancer cells (Costa da Silva et al., 2017). The accumulation of iron ions in macrophages increased intracellular iron levels, promoting the pro-inflammatory phenotype (Costa da Silva et al., 2017). Zhang *et al.*, (Zhang et al., 2020) evaluated whether IONPs with different charges have impact on reprogramming TAMs. Macrophages treated with positively charged IONPs and negatively charged IONPs significantly induced tumor retardation, indicating successful repolarization of tumor macrophages (Zhang et al., 2020). Unlike other studies that considered nanoparticles only as an antitumor drug vehicle, these studies suggest that the modulation of TAMs functions by IONPs could be an important tool for breast cancer immunotherapy.

In most studies, *in vitro* screening of antitumor therapeutic compounds is performed in 2D models. This approach has several strengths and has in the past contributed significantly to increase our knowledge of tumor biology. However, assays related to the repolarizing effect of a compound on macrophages as a therapeutic effect in the context of cancer cannot be adequately studied in 2D models, since they do not take into account the complexity and heterogeneity of clinical tumors (Madsen et al., 2021; Zanoni et al., 2016). Three-dimensional (3D) culture models such as multicellular spheroids (MCTS), have been proposed as an alternative approach for the evaluation of the real therapeutic potential of nanomedicines. MCTS models are indeed able of recapitulating some key features of solid tumors, thus representing a valuable tool for a more accurate preclinical screening of nanomedicines (Lazzari et al., 2017). Therefore, the aim of the present work was to evaluate the ability of polyaniline-coated maghemite (Pani/γ-Fe_2O_3) nanoparticles to modulate human macrophages in 2D monolayers and 3D multicellular breast cancer models towards an immunostimulatory profile.***

2. Material and methods

2.1. Polyaniline-coated maghemite nanoparticles (Pani/γ-Fe_2O_3 NPs) preparation and characterization.

Polyaniline-coated maghemite nanoparticles (Pani/γ-Fe_2O_3) nanoparticles were prepared by co-precipitation method as previously described (da Silva et al., 2019). First, the γ-Fe_2O_3 nanoparticles were produced through a chemical co-precipitation method and, subsequently, coated with the conducting polymer via chemical emulsion polymerization of the aniline monomer. Initially, 50 mL of two sources of iron (1 M $FeCl_2{\cdot}4H_2O$ and 2 M $FeCl_3{\cdot}6H_2O$ in aqueous solution) were added to a 250 mL round-bottom flask, and the mixture kept under strong magnetic stirring for 10 min. Subsequently, was added 125 mL of a 1:1 aqueous NH_4OH solution. After allowing the reaction to proceed for 2 h, the γ-Fe_2O_3 nanoparticles were confined to the bottom of the tube with the help of a magnet and washed with ultrapure water for the removal of impurities. The product was dried in an oven at 50 °C for 48 h and grounded in a mortar.

For the envelopment of the iron oxide nanoparticles by Pani chains, was added 100 mL of a 0.1 M hydrochloric acid (HCl) solution to a round bottom flask, which was placed under magnetic stirring. Then, sodium dodecyl sulfate (SDS) and γ-Fe_2O_3 nanoparticles were consecutively added to the flask and allowed to disperse for 5 min, before 136 μL of the aniline monomer was added to the flask. For complete polymerization, 40 mg of ammonium persulfate (APS) was dissolved in 20 mL of a 0.1 M HCl solution and added to the flask, which was stirred for 24 h. The resulting material was washed three times with methanol and, subsequently, three times with ultrapure water. Finally, Pani/γ-Fe_2O_3 nanoparticles was dried in an oven at 50 °C for 24 h and grounded in a mortar.

To be used in *in vitro* assays, nanoparticles were suspended in type I water at a concentration of 3 mg/mL and subjected to a sterilization procedure at 121 °C, 1 atm for 18 min. After the sterilization the nanoparticles were characterized according with the next topics.

The presence of endotoxins in iron oxide nanoparticles can promote the polarization of macrophages from the M2-like phenotype to M1-like. Therefore, endotoxin levels in nanoparticles were quantified using the Pierce™ LAL (Limulus Amebocyte Lysate) Chromogenic Endotoxin Quantitation kit (Thermo Scientific), according to the manufacturer's protocol. Initially, a standard curve was prepared with concentrations of 1, 0.5; 0.25 and 0.1 EU/mL endotoxin. For the procedure, half area microplates (Corning) were placed in a dry bath (Fisher Scientific) for 10 min at 37 °C. Then, 25 μL of each standard and Pani/γ-Fe_2O_3 nanoparticles at concentrations of 0.001; 0.01 and 0.1 mg/mL were added to wells of the plate in triplicate, the plates were sealed and incubated for 5 min at 37 °C. After the incubation, 25 μL of limulus amebocyte lysate was added to each well, the plates were resealed, shaken for 10 min and incubated for 10 min at 37 °C. Then, 50 μL of substrate solution was added to each well, the plates were sealed, gently shaken for 10 min and incubated for more 10 min at 37 °C. Finally, 25 μL of stop solution was added to each well, the plates were sealed and gently shaken for 10 min. Standard endotoxin and nanoparticles were prepared by dilution in endotoxin-free water. The reading was performed at 410 nm on a Spectramax 340pc plate reader (Molecular Devices).

Pani/γ-Fe_2O_3 nanoparticles were characterized in terms of their morphology and size by transmission electron mic maghemite copy (Tecnai Spirit G2). Nanoparticles average size was calculated by the average of two diameters measurements per nanoparticle, evaluated in at 300 different particles using ImageJ 1.43 software. The hydrodynamic size, polydispersion index and zeta potential were analyzed by dynamic light scattering (DLS) in Litesizer™ 500 (Anton Paar). The functional groups present in Pani/γ-Fe_2O_3 nanoparticles were investigated by using the Fourier transform infrared spectroscopy (FTIR) in FTIR-8400S (Shimadzu). The samples were prepared with potassium bromide pellet (KBr) and the spectra were obtained in the range of 4000 to 400 cm^{-1}.

2.2. Ethics statement

Human samples were obtained in agreement with the principles of the Declaration of Helsinki. Monocytes were isolated from surplus buffy coats from healthy blood donors, kindly provided by the Immunohemotherapy Department of Centro Hospitalar Universitário São João (CHUSJ), Porto, Portugal. Procedures were approved by the Centro Hospitalar Universitário São João Ethics Committee (protocol 90/19).

2.3. Cells and culturing

MCF-7 human breast cancer cells were kindly provided by Dr. Meriem Lamghari (i3S, Porto, Portugal). Cells were cultured in Dulbecco's Modified Eagle's Medium/Nutrient Mixture F-12 (DMEM/F12) (Gibco), supplemented with 10% of heat inactivated fetal bovine serum (FBS), penicillin (100 IU/mL) and streptomycin (100 mg/mL), and incubated in 5% CO_2 and 95% relative humidity at 37 °C. Human mammary fibroblast (hMF) were kindly provided by Dr. Sílvia Bidarra (i3S, Porto, Portugal). Cells were cultured in DMEM High Glucose with UltraGlutamine (Lonza), supplemented with 10% of heat inactivated FBS (Gibco), penicillin (100 IU/mL) and streptomycin (100 mg/mL) (Sigma), and incubated in 5% CO_2 and 95% relative humidity at 37 °C. Human monocytes were isolated from buffy coats from healthy blood donors using RosetteSep-Human Monocyte Enrichment Cocktail kit (StemCell Technologies), according to manufacturer's instructions. Monocytes were cultivated in RPMI (Gibco) supplemented with 10% of heat inactivated FBS Premium (South America) (Biowest), penicillin (100 IU/mL) and streptomycin (100 mg/mL), and incubated in 5% CO_2 at 37 °C. For monocyte differentiation to macrophage, monocytes were incubated for 10 days in RPMI supplemented with 10% of heat inactivated FBS Premium (South America) (Biowest), penicillin (100 IU/mL) and streptomycin (100 mg/mL), and incubated in 5% CO_2 and 95% relative humidity at 37 °C.

2.4. Nanoparticles biocompatibility in 2D

The biocompatibility of the Pani/γ-Fe_2O_3 nanoparticles in MCF-7, hMF, monocytes and macrophages was measured by a resazurin assay. For MCF-7, hMF and monocytes 1×10^4 cells per well were seeded in 96-well plates and allowed to attach overnight. After that, the medium was removed and concentrations ranging from 50 to 400 μg/mL of Pani/γ-Fe_2O_3 nanoparticles suspension in complete medium (300 μL) were added to the cells and incubated for 24 h and 72 h, at 37 °C under 5% CO_2. At each time-point, the medium was removed and 300 μL of resazurin 10% (v/v) in complete media were added to each well and incubated for 2 h at 37 °C in the dark.

To assess the biocompatibility of the macrophages, 2×10^5 monocytes per well were seeded in 24-well plate with cover slips in complete RPMI medium and incubated for 10 days in 5% CO_2 at 37 °C to allow the differentiation into macrophages. After, cells were treated in the same manner as MCF-7, monocytes and hMF.

All data was normalized related to the control without treatment (complete medium), which was considered 100% viability. Fluorescence was measured at the excitation and emission wavelengths of 530 nm and 590 nm, respectively, using a SynergyMx™ MultiMode Microplate Reader (BioTek™, USA). All samples were done in triplicate.

2.5. Macrophage polarization in 2D cultures and profile evaluation

For monocyte-macrophage differentiation, 2×10^5 cells were cultured in 24-wells plate with cover slips for 10 days in complete RPMI1640 medium. For M1 and M2 macrophages (polarization controls), macrophages were incubated with 10 ng/mL LPS (Sigma-Aldrich) or IL-10 (ImmunotoTools), respectively, for 72 h. Unstimulated macrophages were used as controls. For the treatment, Pani/γ-Fe_2O_3 nanoparticles (50 μg/mL) were added to IL-10-stimulated macrophages after 4 h of IL-10 stimulation follow by 72 h of incubation. In addition, Pani/γ-Fe_2O_3 NPs (50 μg/mL) were added to macrophages without IL-10 and LPS stimulation for 72 h.

For cell surface receptor expression analysis, macrophages were incubated with Accutase (eBioscience) at 37 °C during 30 min and harvested by gently scrapping. Cells were washed and resuspended in FACS buffer (PBS, 2% FBS (Biowest), 0.01% sodium azide) containing appropriate conjugated antibodies, and stained in the dark for 40 min at 4 °C. Macrophages were immunostained with the antibodies anti-human CD14-APC (1:25) (Immunotools, clone BU63), anti-CD86 (1:25) (Immunotools, clone BU63) and anti-CD163 (1:10) (BD Biosciences, clone GHI/61). After additional washing steps, cells were acquired on a Accuri Flow Cytometer (BD Biosciences). All data was processed with FlowJo software (Tree Star, Inc.).

2.6. Multicellular tumor spheroids (MCTS) formation

MCTS were formed as previously established in the group (unpublished data) using commercially available micro-molds (3D Petri Dish®, from MicroTissues Inc.). First, agarose (2%, w/v) was dissolved in NaCl (0.9%, w/v) solution and casted into micro-molds to form molds with 81 wells. Next, the molds were placed in 12-well plates and RPMI media (2 mL) was added to each well to equilibrate the molds for 24 h. Afterwards, cells suspension, corresponding to 5000 total cells per MCTS (190 μL), were added to the molds and allowed to settle for 30 min before adding media (2 mL) to each well. MCTS were produced in double culture (MCF-7 and monocytes) and triple culture (MCF-7, hMF and monocytes), keeping the total number of cells per MCTS at 5000 cells, ratio 1:2 for double culture (MCF-7: Monocytes) and ratio 1:2:1 for

triple culture (MCF-7: Monocytes: hMF). Then, the plate was incubated at 37 °C and 5% CO_2 for 7 days.

2.7. Multicellular tumor spheroids characterization

After 7 days of incubation, double and triple MCTS were characterized by size, cell metabolic activity and histological analysis. The images were taken using a Brightfield microscopy (ZOE™ Fluorescent Cell Imager, Bio-Rad Laboratories). The average size of each condition was calculated by performing the average of two diameters measurements per MCTS, evaluated in at least five different MCTS using ImageJ 1.43 software.

The metabolic activity of MCTS was measured by resazurin assay. Briefly, RPMI containing 20% resazurin (v/v) was added to each well containing one micro-molds with 81 MCTS and incubated in the dark at 37 °C for 2 h. After incubation, the media was transferred to a 96-well black plates, and the fluorescence was measured at the excitation and emission wavelengths of 530 nm and 590 nm, respectively, using a SynergyMx™ MultiMode Microplate Reader (BioTek™).

For histological analysis, the media was removed from the wells and MCTS were fixed in 4% of Paraformaldehyde (PFA). Afterwards, the molds were washed three times with PBS and agarose 1% (w/v) was added to the top of each mold to fix spheroids into the molds. The molds were then embedded in paraffin using an automated embedding system (Thermo Scientific™ STP 120 Spin Tissue Processor). Paraffin embedded samples were sectioned into 3 μm sections, deparaffinized in xylene and rehydrated in graded alcohol series. Staining was performed with Hematoxylin and Eosin.

2.8. Nanoparticles biocompatibility on 3D MCTS

The biocompatibility of Pani/γ-Fe_2O_3 NPs on MCTS was evaluated by resazurin assay. First, double and triple culture MCTS were cultured for 7 days in 12-well plates, as described above. After 7 days of incubation, ranging from 50 to 400 μg/mL of Pani/γ-Fe_2O_3 nanoparticles suspension in complete medium (2 mL) were added to the cells and incubated at 37 °C for 72 h. After incubation, the medium was removed and 2 mL of 20% resazurin (v/v) was added to each well and incubated in the dark at 37 °C for 2 h. Then, the media was transferred to a 96-well black plates, and the fluorescence was measured fluorescence was measured as described in topic 2.4.

2.9. 3D cellular interaction with Pani/γ-Fe_2O_3 nanoparticles

Double and triple culture MCTS were cultured for 7 days in 12-well plates, as described above. At day 7, the spheroids were treated with 0.1 mg/mL of Pani/γ-Fe_2O_3 NPs for 72 h and then collected from the wells to 15 mL tubes. For the ultrastructure analysis, cells were fixed in a solution of 2.5% glutaraldehyde with 2% formaldehyde in 0.1 M sodium cacodylate buffer (pH 7.4) for 1 h, at RT, and post fixed in 1% osmium tetroxide diluted in 0.1 M sodium cacodylate buffer. After-centrifugation, the pellet was resuspended in Histogel™ (Thermo, HG-4000-012) and then stained with aqueous 1% uranyl acetated solution overnight, dehydrated and embedded in Embed-812 resin. Ultra-thin sections (50 nm thickness) were cut on a RMC Ultramicrotome (PowerTome, USA) using Diatome diamond knifes, mounted on mesh copper grids, and stained with uranyl acetate substitute and lead citrate for 5 min each. Samples were viewed on a JEOL JEM 1400 transmission electron microscope (JEOL, Tokyo, Japan) and images were digitally recorded using a CCD digital camera Orius 1100 W (Tokyo, Japan). The transmission electronic microscopy was performed at the HEMS core facility at i3S, University of Porto, Portugal.

2.10. Macrophage polarization on 3D model

Double and triple MCTS were cultured for 7 days in 12-well plates. After that, the medium was removed from the wells and the cells were treated as described below. For M1 and M2 macrophage polarization controls, MCTS molds were incubated with 10 ng/mL LPS (Sigma-Aldrich) or IL-10 (ImmunotoTools), respectively, for 72 h. For treatment evaluation, Pani/γ-Fe_2O_3 nanoparticles (100 μg/mL) were added to macrophages stimulated with IL-10 after 4 h, for an additional 72 h. Pani/γ-Fe_2O_3 nanoparticles (100 μg/mL) were added to macrophages for 72 h, and controls were left unstimulated. After, MCTS (81 spheroids per sample) were collected to 15 mL Falcon tube, dissociated to single cell suspension using warm Versene solution (Gibco) for 10 min at 37 °C and warm Accutase solution (eBioscience) for 5 min at 37 °C until a homogeneous single cell suspension was observed. The cells were washed twice with PBS containing 2% of FBS and resuspended and transferred to a round-bottom 96 well plate. Next, cells were resuspended in a solution of PBS containing 2% of FBS with anti-CD14 (1:25) (Immunotools, clone MEM-18), anti-CD86 (1:25) (Immunotools, clone BU63) and anti-CD163 (1:10) (BD Biosciences, clone GHI/61); antibodies and incubated (40 min, 4 °C) in the dark. After first incubation, cells were washed twice with PBS containing 2% FBS and resuspend in Fixable Viability Dye eFluor™ 780 (1:10000) (Invitrogen™, eBioscience) solution follow by incubation for more 30 min at 4 °C in the dark. The samples were washed twice using PBS containing 2% of FBS and resuspend in 1% PFA in PBS containing 2% of FBS. Samples were analyzed with BD FACSCanto™ II flow cytometer (BD Biosciences). All data was processed with FlowJo software (Tree Star, Inc.).

2.11. Statistical analysis

All statistical analyses were performed using GraphPad Prism version 6.04 (GraphPad Software). Results are expressed as mean ± standard deviation (s.d.) of at least three independent experiments. Data normality was previously evaluated using the Shapiro-Wilk test. For Gaussian distribution, the ANOVA test was used followed by Dunnett's post-hoc test. Level of significance set at probabilities of $*p < 0.05$.

3. Results

3.1. Pani/γ-Fe_2O_3 nanoparticles characterization

Pani/γ-Fe_2O_3 nanoparticles TEM micrographs and the corresponding particle size distribution histogram are shown in Fig. 1a-b. From the TEM images (Fig. 1A) it was possible to observe two distinct regions in the material: a darker one, corresponding to a γ-Fe_2O_3 core surrounded by a second clearer region associated to the Pani chains. Thus, the morphological images confirm the conclusion derived from the FTIR analyses, that a shell of conducting polymer chains indeed coats the γ-Fe_2O_3 core. The size distribution histogram obtained from TEM (Fig. 1B) and DLS measurements revealed that the composite nanoparticles had an average diameter of 37.87 ± 6.48 nm and clusters hydrodynamic size of 442.78 ± 145.99 nm, polydispersity index 0.4 ± 0.08 and zeta potential of −24.81 ± 0.38 mV. The results showed that Pani/γ-Fe_2O_3 particles have nanoscale dimensions, but they tend to agglomerate and form clusters.

Further, it was performed a FTIR analysis to assess the incorporation of Pani chains in γ-Fe_2O_3 nanoparticles (Fig. 1C). For the polymer Pani, the characteristic peaks are observed at 2925 cm^{-1} and 2856 cm^{-1}, which can be attributed to the C-H_2 bond, symmetrical and asymmetrical elongation, respectively, of the alkyl substituent of the surfactant used in the polymerization reaction, indicating the presence of the polymer (Alves et al., 2012; Sydulu Singu et al., 2011). In the region between 1585 cm^{-1} and 1498 cm^{-1} it is possible to identify the vibrations of stretching C=N and C=C of quinoid and benzene rings, and between 790 and 800 cm^{-1} a peak related to the CH bond of the aromatic ring (Wu et al., 2008; Khan et al., 2010). In addition, it was verified the presence of two peaks at 3858 and 3751 cm^{-1} characteristics of the vibration of NH bond of primary amines, that results in a split

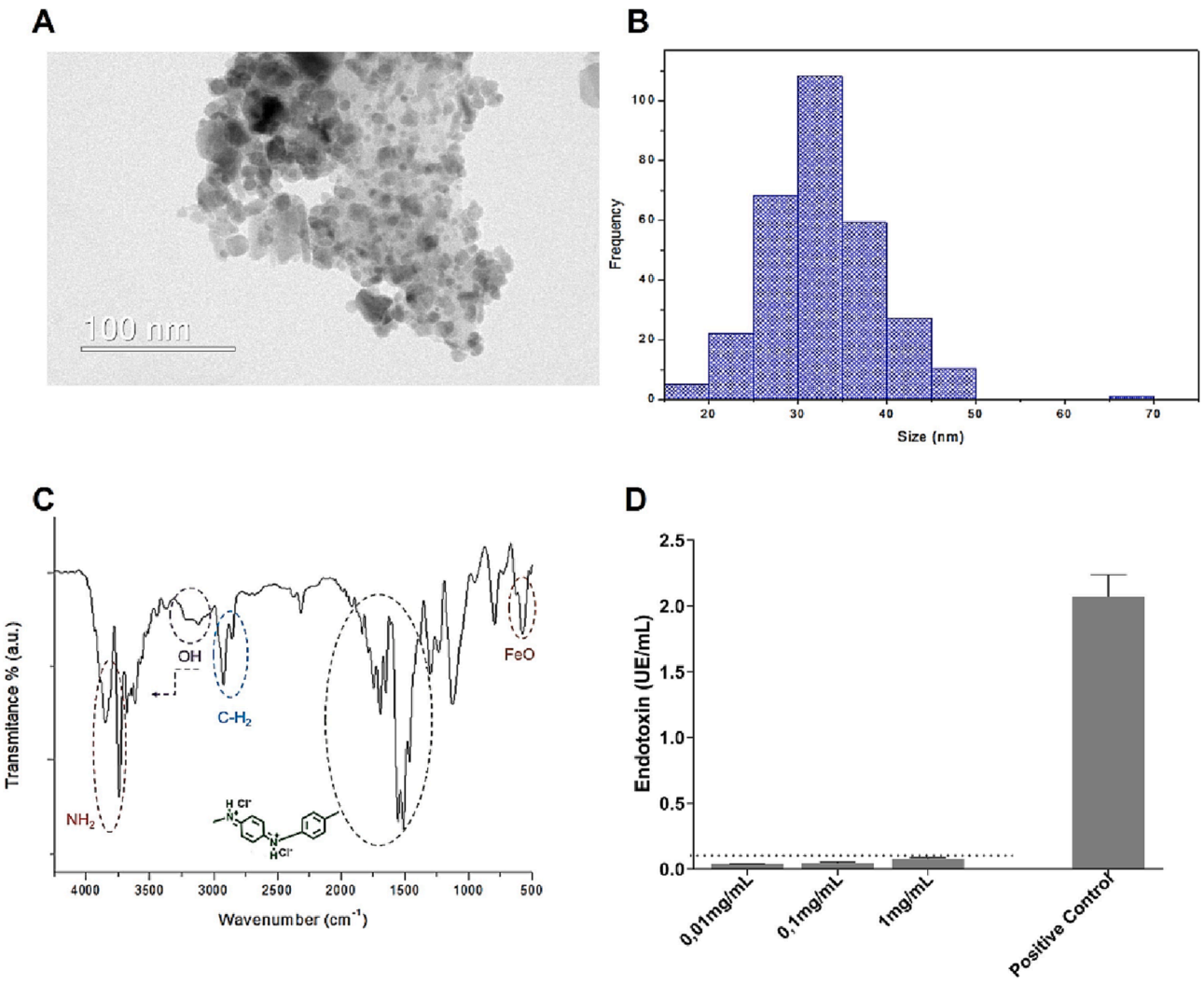

Fig. 1. Characterization of Pani/γ-Fe_2O_3 nanoparticles. a) TEM micrographs of Pani/γ-Fe_2O_3 nanoparticles clusters; b) Mean size distribution histogram of 300 aleatory nanoparticles in different clusters counted in image J software.; c) FTIR spectra of Pani/γ-Fe_2O_3 nanoparticles. We indicate the peaks that are most relevant to our discussion; d) Endotoxin levels in Pani/γ-Fe_2O_3 nanoparticles.

in the region between 1560 and 1640 cm^{-1}. These peaks are strongly present in the polymer of polyaniline. It was also observed at 1306 cm^{-1} peak that can be attributed to the CN amine elongation (Sydulu Singu et al., 2011; Rajendran et al., 2017; Silverstein, 2005; Sim et al., 2015). The peaks between the regions of 3400–3300 cm^{-1} refer to the OH groups present on the surface of the particles and the three descending peaks in the region between 3610 and 3640 cm^{-1} can be associated with the presence of free OH, since the nanoparticles are suspended in water (Silverstein, 2005). The characteristic peak of the F-O bond between the region of 600 cm^{-1} and 440 cm^{-1} was also observed, associated with the intrinsic vibration of the tetrahedral and octahedral sites of the iron oxide crystal (da Silva et al., 2019).

Regarding endotoxin levels, it was observed that Pani/γ-Fe_2O_3 do not present significant amounts of endotoxin for all analyzed concentrations, indicating that Pani/γ-Fe_2O_3 can be used for macrophage reprograming studies (Fig. 1D).

3.2. Biocompatibility of Pani/γ-Fe_2O_3 nanoparticles

To access the biocompatibility of the developed Pani/γ-Fe_2O_3 nanoparticles, the cytotoxicity was evaluated in 2D monolayers and MCTS models by resazurin assay. The monolayers were constituted of MCF-7, hMF, monocytes and macrophages cells after at 24 h and 72 h of incubation. For cytotoxicity analysis we considered the ISO 10993–1100 that discuss about biological evaluation of medical devices for *in vitro* cytotoxicity tests and establish that only reduction of cell viability by more than 30% is considered a cytotoxic effect.

After 24 h of treatment, Pani/γ-Fe_2O_3 nanoparticles were biocompatible for hMF, monocytes e macrophages to all tested concentrations. For MCF-7 cell line, it was observed that nanoparticles did not produce cytotoxicity effect up to 50 μg/mL, while the higher concentrations significantly reduced the cell viability. Regarding 72 h of culture, the results showed that nanoparticles have safety profile up to 50 μg/mL for MCF-7 and monocytes, up to 400 μg/mL for fibroblasts and up to 100 μg/mL for macrophages. Therefore, the nanoparticle concentration of 50 μg/mL was selected for its safety for reprograming macrophage experiments in 2D monolayers.

Regarding the studies of nanoparticle biocompatibility using MCTS models, the results showed that Pani/γ-Fe_2O_3 nanoparticles were not able to induce a reduction of the cell viability in all concentrations evaluated for double MCTS (Fig. 2). However, Pani/γ-Fe_2O_3 nanoparticles have successfully reduced the cell viability of the triple co-culture MCTS. After 72 h of culture, nanoparticles induced an inhibition effect in the concentrations of 100, 200 e 400 μg/mL able of reducing the cell viability by 28 %, 48 % and 33 %, however without statistical significance (ANOVA; $p < 0.05$). The results shown a

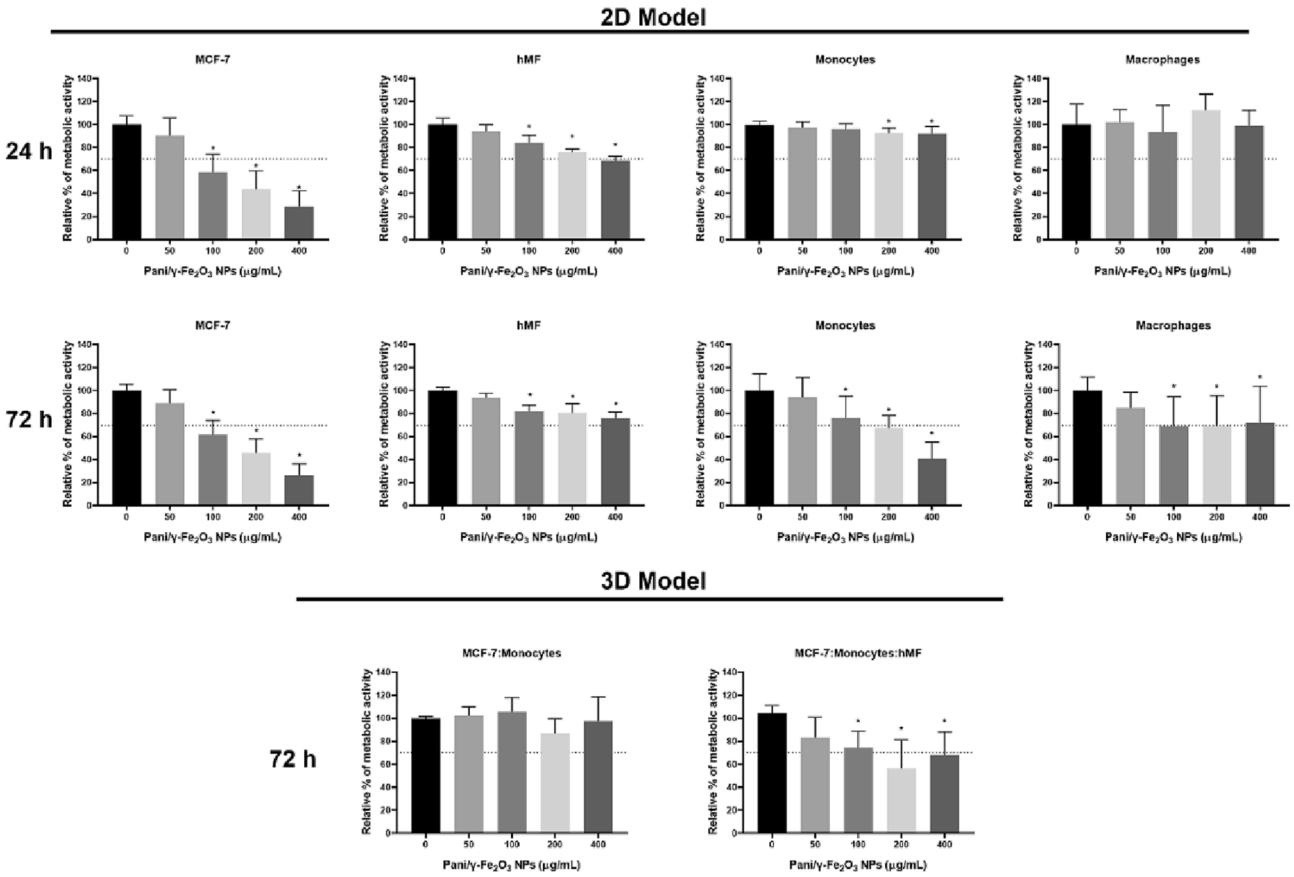

Fig. 2. *In vitro* biocompatibility of Pani/γ-Fe_2O_3 nanoparticles in 2D and MCTS models. Values represent mean ± s.d. (n = 3). Statistical significance was analyzed with analysis of variance (ANOVA) with Dunnett's multiple comparisons test, with the level of significance set at probabilities of $*p < 0.05$. Dotted line represents 70% of cell viability (ISO 10993–1100).

significant reduction in cell viability after the incubation with 100 μg/mL of NPs, but the reduction observed was less than 30%. Thus, the nanoparticle concentration of 100 μg/mL was established for reprograming macrophage experiments in 3D multicellular models. Overall, the enhanced cytotoxic effect of Pani/γ-Fe_2O_3 in triple MCTS comparing to double MCTS may be due to difference in the cellular composition of the MCTs, which can result from different cell-nanoparticles interactions.

3.3. *Pani/γ-Fe_2O_3 nanoparticles inhibit M2 polarization in 2D models*

TAMs represent the major component of many solid tumors and these cells frequently have associated pro-tumoral functions and are functionally similar to M2-like macrophages. Therapies favoring a pro-inflammatory profile M1 might improve conventional anticancer therapies (Genard et al., 2017).

To determine if Pani/γ-Fe_2O_3 nanoparticles have the ability to inhibit M2 polarization and to promote M1 polarization, nanoparticles were added to IL-10-stimulated macrophages and the surface expression of CD86 (M1-like marker) and CD163 (M2-like marker), were evaluated by flow cytometry (Fig. S1; Fig. 3A-C). The resulting adherent cell population predominantly expresses CD14, however it was observed that the treatment with LPS increase the number and mean fluorescent intensity (MFI) of $CD14^+$ cells and the treatment with IL-10 just increase the expression intensity do $CD14^+$ cells, as was already outlined in earlier work (Fig. 3C) (Sandanger et al., 2009; Rahimi et al., 2005). As expected, IL-10 stimulation significantly increased the percentage of $CD163^+$ cells and the treatment with Pani/γ-Fe_2O_3 nanoparticles showed a strong effect in the reduction of percentage of $CD163^+$ cells, suggesting that nanoparticles can prevent macrophage M2-like polarization by IL-10 in 2D cultures (Fig. 3B and 3C). In accordance with that result, it was also observed that Pani/γ-Fe_2O_3 nanoparticles reduced the percentage of $CD163^+$ macrophages in cultures treated only with nanoparticles in relation unstimulated control group (Fig. 3C). The number of $CD86^+$ macrophages also was affected by nanoparticles treatment, but not enough to generate statistical significance, an increase of about 8% in the percentage of $CD86^+$ was observed after the treatment in IL-10-stimulated macrophages (Fig. 3C). Contrary to what we expect LPS stimulation was not able of significantly increase the number of $CD86^+$ cells (Fig. 3C). The median fluorescence intensity (MFI) data (Fig. 3C) agreed with the cell percentage results. Overall, Pani/γ-Fe_2O_3 nanoparticles seemed to prevent M2 macrophage polarization.

3.4. *Characterization of double and triple culture MCTS model*

To select effective therapies, *in vitro* MCTS model including cancer cells, fibroblasts, and monocytes are adequate tools to recapitulate the TME and the phenotype of TAMs *in vitro*. The characterization of the MCTS models, previously established in our group, was started after 7 days of incubation. As observed by brightfield microscopy, the MCTS were spherical and compact structures (Fig. 4a). However, in the double and triple culture, small cellular aggregates were found around of the MCTS, likely corresponding to monocytes which did not penetrate the MCTS. The analysis of MCTS diameter demonstrated an average size of 404.6 ± 16.3 μm for double culture and 456.7 ± 5.7 μm for triple culture (Fig. 4b). Their metabolic activity was measured, double culture showed average activity of 5168.0 ± 221.7 R.F.U and triple culture showed average activity of 6787.0 ± 1447.0 R.F.U (Fig. 4c).

Regarding to histological analyses (Fig. 4d), the seeded cells formed

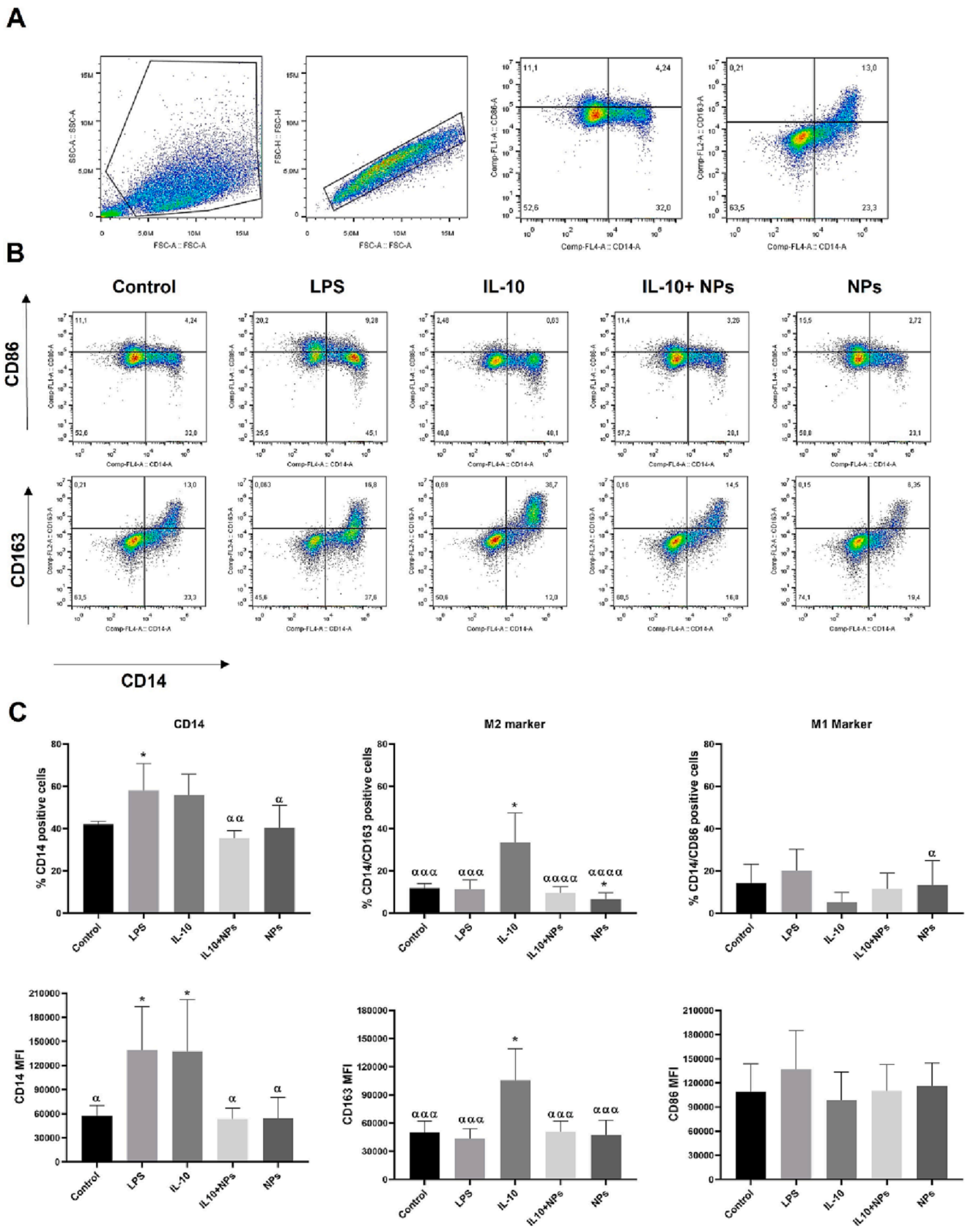

Fig. 3. Reprograming of macrophages by Pani/γ-Fe_2O_3 NPs. A) Flow cytometry gating strategy to study macrophage polarization in the 2D model after 72 h incubation with media (control), LPS, IL-10, IL-10+ NPs and NPs. B) The pseudocolor plot of a representative phenotypic profile show the electronic gate used to identify $CD14^+$ $CD163^+$ cells and $CD14^+$ $CD86^+$ cells gated on single cells. C) Percentage and median fluorescence intensity (MFI) of $CD14^+$ cells, $CD14^+$ $CD163^+$ cells and $CD14^+$ $CD86^+$ cells; Values represent mean ± s.d. (n = 5). Statistical significances were performed using ANOVA test followed by Dunnett's post-hoc test

(*p < 0.05; **p < 0.01; ***p < 0.001 relative to unstimulated macrophages- control; α p < 0,05; αα p < 0.01; ααα p < 0.001 relative to IL-10-stimulated macrophages).

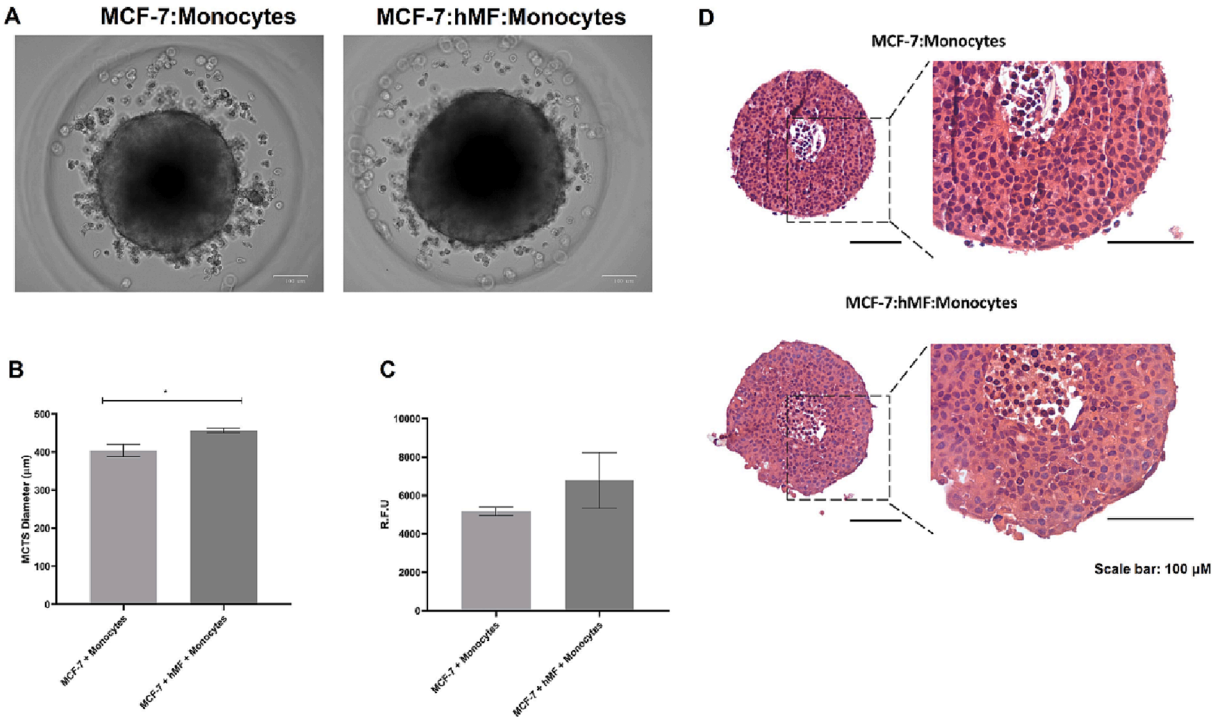

Fig. 4. Comparison between double and triple MCTS. A) Brightfield microscopy images of the morphology of the double and triple co-culture. Scale bars represent 100 µm; B) Double and triple MCTS diameter; C) Double and triple metabolic activity; D) H&E staining of the double (MCF-7: Monocytes) and triple MCTS (MCF-7: hMF: Monocytes) (and respective magnification, portrayed). Scale bars represent 100 µm. e) Immunofluorescence microscopy images of double and triple MCTS. Values represent mean ± s.d. (n = 3). Statistical significance was analyzed using Unpaired *t* test, with the level of significance set at probabilities of $^{*}p < 0.05$.

compact and spherical MCTS. Furthermore, after 7 days of culturing, the MCTS developed a necrotic core as seen by the presence of condensed chromatin and nuclear disintegration. However, comparing to the double and triple culture MCTS, the introduction of hMF in MCTS model resulted in some loss of structure, the triple MCTS is less compact than the double model. This structural difference may interfere in the penetration of agents into the model system, such as resazurin solution and nanoparticles. In agreement with structural results presented, it was observed that double MCTS model showed less interaction with resazurin solution and/or nanoparticles, affecting biocompatibility and macrophage polarization results. The biocompatibility results of nanoparticles in 2D culture were more similar to triple MCTS model than those obtained in double MCTS model, indicating changes in the interaction of this double MCTS models with the nanoparticles.

3.5. *Internalization of Pani/γ-Fe_2O_3 nanoparticles by macrophages of MCTS model*

The ability of macrophages inside of double and triple MCTS to internalize and interact with Pani/γ-Fe_2O_3 nanoparticles was determined by TEM. Fig. 5 shows that the spheroids maintained their spherical shape after nanoparticle exposure. In the sections that we analyzed, the most part of monocyte/macrophages was localized in the peripheral region of the spheroids. In addition, it was possible to observe junctions between MCF-7 and fibroblast, which confirm the communication between these cell types and demonstrate the success in the establishment of MCTS model (Fig. 5A). Pani/γ-Fe_2O_3 nanoparticles were preferentially located in the outer layers of the spheroid, in the most part inside of the macrophages. In macrophages, the close-up TEM view revealed the presence of Pani/γ-Fe_2O_3 nanoparticles in cell endosome-like structures or distributed throughout the cytosol (Fig. 5B). These results confirm that nanoparticles interact with macrophages in a 3D model and are degraded in endosomes.

3.6. *Macrophage polarization on MCTS models by Pani/γ-Fe_2O_3 NPs*

Due to the importance of macrophages in the TME, in this study it was analyzed if Pani/γ-Fe_2O_3 NPs could influence the polarization of macrophages towards a more anti-tumor profile (M1) in 3D multicellular model composed of fibroblasts, MCF-7 cells and monocytes/macrophages. The concentration of Pani/γ-Fe_2O_3 NPs for the treatment of MCTS models was 100 µg/ml, since the reduction in the cell viability after the treatment with this NPs concentration was less than 30% in the biocompatibility study (Fig. 2). For this purpose, double and triple co-culture MCTS were stimulated with IL-10 for 4 h follow by treatment with Pani/γ-Fe_2O_3 NPs for 72 h. After that, MCTS were collected, dissociated into single cell suspension and the $CD14^{+}$ macrophage population was analyzed for the expression of CD163 and CD86 receptors by flow cytometry (gate-strategy - Fig. S2 and S3).

Regarding the double model (MCF-7: Monocytes), the stimulation with IL-10 significantly increased in the percentage of $CD163^{+}$ macrophages and decreased the number of $CD86^{+}$ macrophages, indicating that IL-10 stimulation is able to promote an anti-inflammatory phenotype in macrophages present in this 3D model (Fig. 6A and B). As seen in the 2D culture containing only macrophages, about the results of MFI, it was verified that the IL-10 treatment increased $CD14^{+}$ intensity expression, and the NPs addition was able to restore the $CD14^{+}$ expression to values like those obtained in the control group (Fig. 6B). In relation to the impact of Pani/γ-Fe_2O_3 NPs on the macrophage polarization in the double model, the addition of NPs was not able to affect the

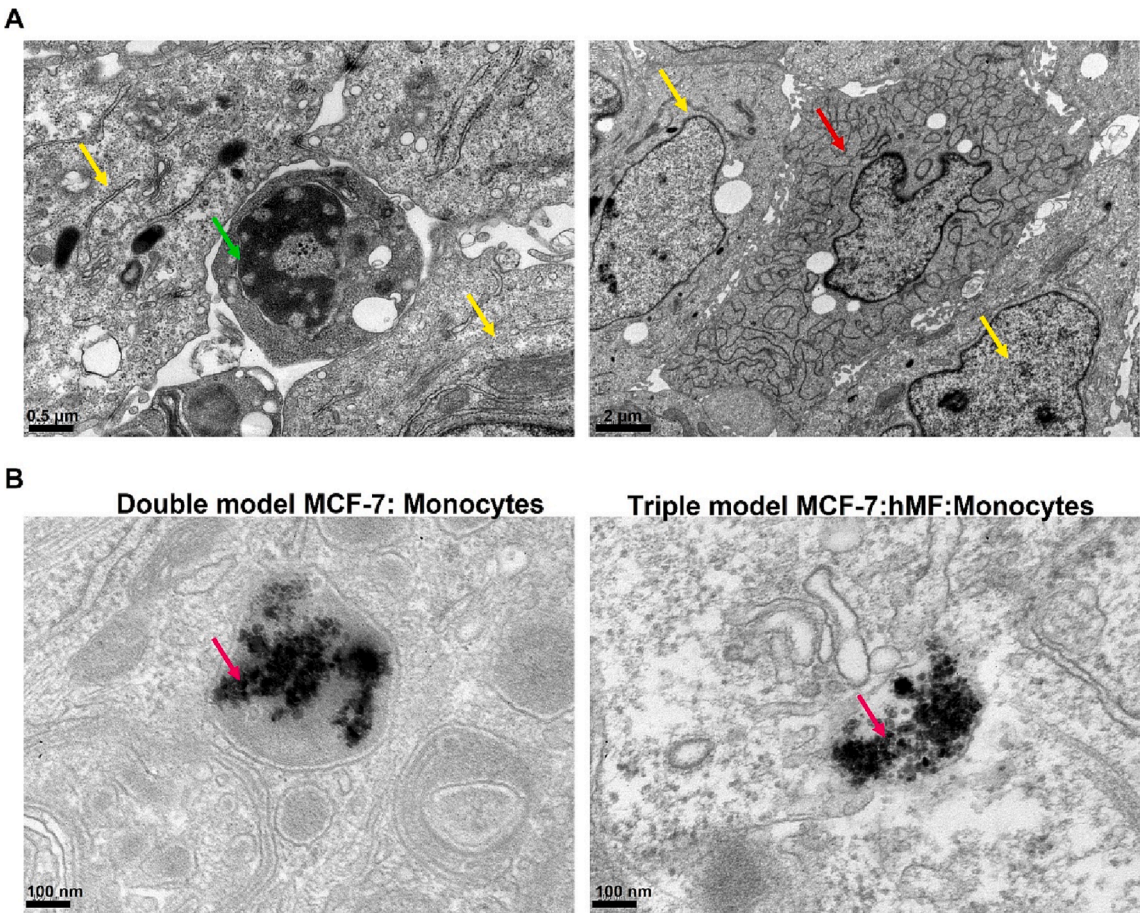

Fig. 5. Transmission electron microscopy (TEM) image of double and triple MCTS treated with Pani/γ-Fe_2O_3 NPs. a) Morphology of the cells present in the MCTS models: MCF-7 (yellow arrow), fibroblasts (red arrow) and macrophages (green arrow); b) Pani/γ-Fe_2O_3 NPs were mainly observed in endosome-like structures of double and triple model (black points and pink arrow). The black bars indicate scale. (For interpretation of the references to colour in this figure legend, the reader is referred to the web version of this article.)

percentage of $CD14^+$, $CD163^+$ and $CD86^+$ cells neither their intensity expression after 72 h of treatment in conditioned IL-10 macrophages (Fig. 6B). Regarding the viability of the cancer cells ($CD14^-$) and macrophages ($CD14^+$), no differences upon treatments were observed (Fig. 6C). Overall, the treatment with NPs seems not affect the percentage of M1 and M2 markers of macrophages in the times and conditions analyzed (Fig. 6B).

For the triple model (MCF-7: hMF: Monocytes), it was observed that the treatment with IL-10 curiously did not significantly impact the percentage of $CD163^+$ monocytes/macrophages, but it was able to decrease the percentage of $CD86^+$ monocytes/macrophages (Fig. 7A and B). Further, IL-10 stimulation also increased $CD14^+$ intensity expression (MFI) and the nanoparticles addition restored the $CD14^+$ cells intensity expression to values similar to control group (Fig. 7B). Regarding CD163 expression, was verified that Pani/γ-Fe_2O_3 NPs treatment decreased the percentage of $CD163^+$ cells in relation the control group (Fig. 7B). In triple MCTS model IL-10- stimulated and treated with nanoparticles was verified decrease of about 5% in the proportion of $CD163^+$ macrophages, but not enough to generate statistical significance. Also was observed that Pani/γ-Fe_2O_3 NPs treatment increase in 16% the number of $CD86^+$ cells after 72 h in IL-10-stimulated macrophages. The addition of nanoparticles did not significantly reduce the percentage of $CD163^+$ cells, showing that Pani/γ-Fe_2O_3 NPs may have an immunopotentiation role in the macrophages polarization to M1-like profile in more complex culture systems than inhibit M2 polarization in MCTS models (Fig. 7B). Regarding the viability of the cancer cells and macrophages, no differences upon treatments were observed as in double model (Fig. 7C). Overall, despite the slight impact of NPs in the polarization markers analyzed, this model constitutes an interesting screening platform to test different formulations with impact on cancer but also stromal cells, since it is an *in vitro* model mimicking the characteristics of the tumor microenvironment, resulting in the presence of several molecules and conditions that affect the tumor microenvironment and the tumor growth than in 2D cultures.

4. Discussion

Nanoparticles have been extensively studied to modulate cells of the innate immune system to increase the anticancer response. In particular, the development of iron oxide nanoparticles as a tool for the regulation of macrophage polarization may represent a promising immunotherapeutic strategy against breast cancer. In this study, it was described the use of Pani/γ-Fe_2O_3 NPs as a potential platform for modulating macrophages to pro-inflammatory and tumor suppressor phenotype in TME. Based on previous studies, iron oxide nanoparticles have been successfully used as immunopotentiators for the treatment of various types of cancer, through the modulation of M1 macrophage profile to M2 macrophage profile (Zanganeh et al., 2016; Costa da Silva et al., 2017; Zhou et al., 2020; Li et al., 2019).

Macrophage polarization is closely associated with differential regulation of iron metabolism due to their differential expression of related molecules involved in iron uptake, storage and release (Zhu et al., 2015). Macrophage iron homeostasis is linked to their functional heterogeneity as well as their extreme roles during inflammation (Jung

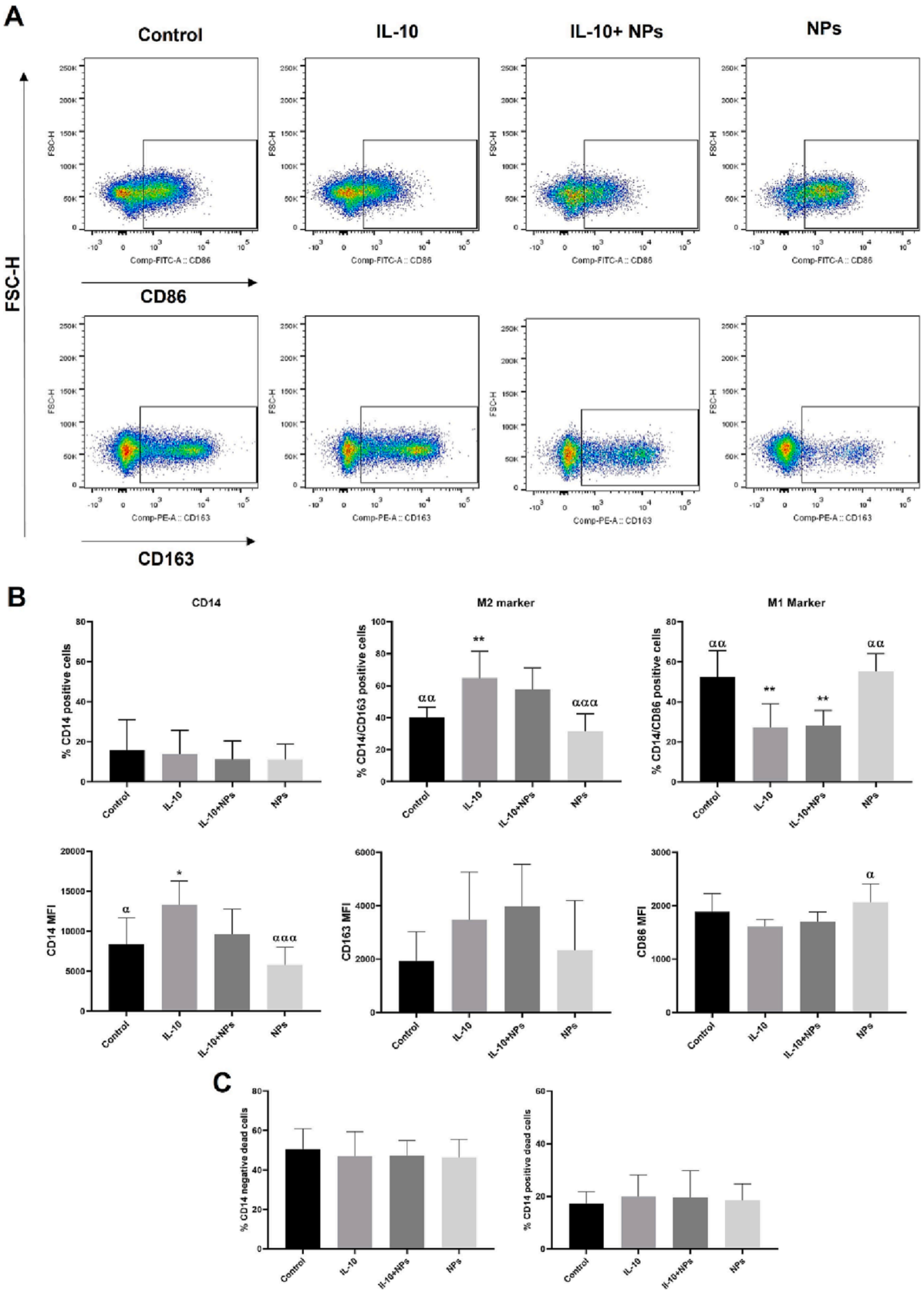

Fig. 6. Reprograming of macrophages on double MCTS by Pani/γ-Fe_2O_3 NPs. A) The pseudocolor plot of a representative phenotypic profile show the electronic gate used to identify $CD14^+$ cells gated on single cells, and $CD163^+$ cells and $CD86^+$ cells gated on $CD14^+$ cells of the double model. B) Percentage and MFI of CD14+, $CD163^+$ cells and $CD86^+$ cells in double model; C) Percentage of $CD14^+$ dead cells and percentage of $CD14^-$ dead cells in double model. Values represent mean ± s.d. (n = 6). Statistical significances were performed using ANOVA test followed by Dunnett's post-hoc test (*$p < 0.05$; **$p < 0.01$; ***$p < 0.001$ relative to unstimulated macrophages- control; α $p < 0,05$; αα $p < 0.01$; ααα $p < 0.001$ relative to IL-10-stimulated macrophages).

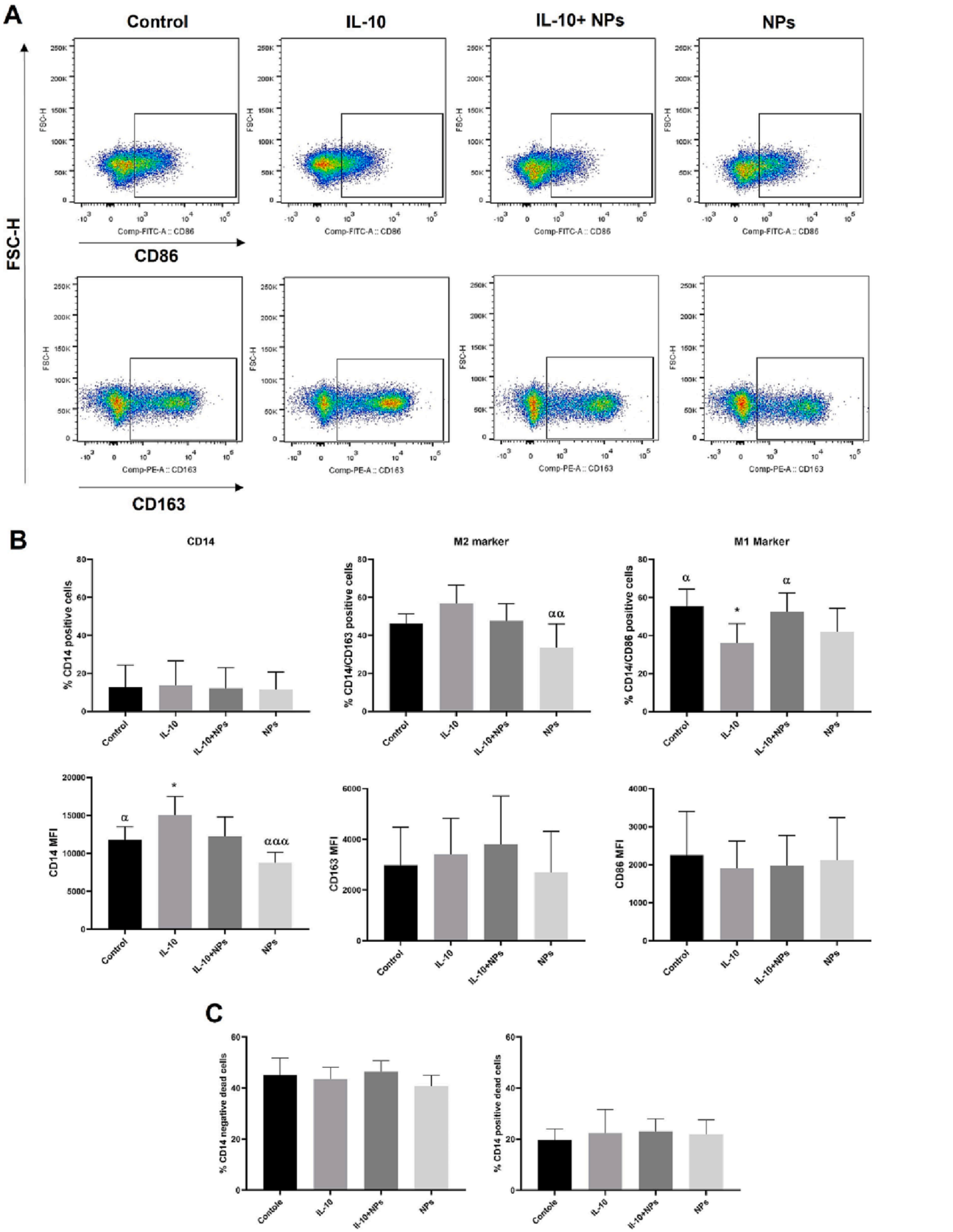

Fig. 7. Reprograming of macrophages on triple MCTS by Pani/γ-Fe_2O_3 NPs. A) The pseudocolor plot of a representative phenotypic profile show the electronic gate used to identify $CD14^+$ cells gated on single cells, and $CD163^+$ cells and $CD86^+$ cells gated on $CD14^+$ cells of the triple model. B) Percentage and MFI of CD14+, $CD163^+$ cells and $CD86^+$ cells in triple model; C) Percentage of $CD14^+$ dead cells and percentage of $CD14^-$ dead cells in triple model. Values represent mean ± s.d. (n = 6). Statistical significances were performed using ANOVA test followed by Dunnett's post-hoc test (*$p < 0.05$; **$p < 0.01$; ***$p < 0.001$ relative to unstimulated macrophages- control; α $p < 0,05$; αα $p < 0.01$; ααα $p < 0.001$ relative to IL-10-stimulated macrophages).

et al., 2015). M1-like macrophages have an iron-sequestering phenotype, basically they use iron to generate an acute inflammatory signaling response that this is associated with ROS generation to limit tumor progression (Sacco et al., 2021). M2-like macrophages phenotype display an iron-releasing phenotype characterized by promoting iron recirculation in the TME and supporting tumor cell proliferation, angiogenesis, and metastasis (Sacco et al., 2021).

Our results showed that Pani/γ-Fe_2O_3 NPs have low toxicity to cells under study with endosomal uptake by macrophage. MCF-7 cancer cells were more sensitive to exposure to Pani/γ-Fe_2O_3 NPs than the monocytes and macrophages. The high iron exposure can induce cell death by ferroptosis, which is a form of non-apoptotic cell death characterized by accumulation of lipid peroxides (Recalcati and Cairo, 2021; Lei et al., 2019). However, in macrophages, the pentose phosphate pathway that generates NADPH is particularly active and represents an important cofactor in the production of both toxic oxidants and antioxidants, such as glutathione (GSH) and thioredoxin, which limit oxidative damage (Lei et al., 2019). In this context, the iron content of macrophages is important for their greater resistance and viability to iron exposure and justifies their greater compatibility with the nanoparticles used in this study.

In addition, the data showed that Pani/γ-Fe_2O_3 NPs is able to successfully shape the macrophage immune response *in vitro* in 2D culture systems, reducing the percentage of M2 $CD163^+$ macrophages and increasing the percentage of M1 $CD86^+$ macrophages. This finding has already been seen in other studies that used iron oxide nanoparticles for macrophage reprogramming as an antitumor strategy (Laskar et al., 2013; Zanganeh et al., 2016; Zhang et al., 2020; Kao et al., 2020; Okazaki et al., 2020; Li et al., 2019). The antitumor effect is attributed to the accumulation of intracellular iron in macrophages, promoting transcriptional reprogramming of macrophage phenotypes (Nascimento et al., 2021). The process starts with the interaction between iron oxide nanoparticles and macrophage surface receptors. In general, the pro-inflammatory potential of iron oxide nanoparticles is mediated by pattern recognition receptors expressed on innate immune cells, including Toll-Like Receptors, complement receptors and scavenger receptors, which are involved in downstream MAPK/mTOR cascades and transcription factors – STATs, NF-κB and IRFs, which regulate immune activation and the inflammatory response (Dukhinova et al., 2019). It has also been shown that high intracellular iron concentration can activate NF-κB and induce pro-inflammatory pathways initiating macrophage reprogramming to a pro-inflammatory phenotype associated with the expression of TNF-α and other pro-inflammatory cytokine (Zhao et al., 2018).

The potential clinical applications of pro-inflammatory immune responses mediated by Pani/γ-Fe_2O_3 NPs may assist in potentiating the efficacy of other M1-activating cancer immunotherapies. To assess the potential of Pani/γ-Fe_2O_3 NPs as a strategy for macrophage reprogramming for a pro-inflammatory tumor suppressor profile, it was evaluated their action in MCTS models, also known as 3D *in vitro* models, which can mimic the microenvironment of solid tumors. The 3D multicellular model can mimic the specificity of tissues better than cells grown in monolayers, recapitulating these physiological cell-cell and cell-extracellular matrix interactions (Lu and Stenzel, 2018). However, some points need to be considered when interpreting the results between 2D and 3D models, since the interaction can occur predominantly at the periphery of the spheroid, while only a small penetration of the nanoparticles occurs in the center (Han et al., 2021). It is necessary to take into account that both models assess nanoparticles capture while only the 3D considers the diffusion of nanoparticles (Lu and Stenzel, 2018). The characterization results of double and triple spheroids shown that co-culture between tumor cells, fibroblasts and monocytes increased the diameter and metabolic activity of the spheroid, as well as reduced its compaction but without loss of stability. Studies show that the addition of fibroblasts in 3D models increases the expression of matrix metalloproteinases (MMPs) (Sirén et al., 2006). These proteins, MMPs, are considered the major pericellular proteolytic executors, with a function related to the degradation of the extracellular matrix (ECM) for cell growth, differentiation, survival and tumor cell motility (Itoh and Nagase, 2002). In addition to ECM components, MMPs are able to cleave and process serpins, complement factors, various receptors and adhesion molecules on cell surfaces (McCawley and Matrisian, 2001). In this way, the addition of fibroblasts and macrophages in a 3D architecture replicate the natural TME in terms of physiologically relevant cell-cell communication, nutrient gradients, drug penetration and hypoxic tumor regions (Kuen et al., 2017). Furthermore, tumor-associated fibroblasts are an important component of the TME, playing a role in cancer progression and drug response (Jeong et al., 2016).

The results of biocompatibility found in relation Pani/γ-Fe_2O_3 NPs to the triple MCTS model composed of MCF-7, fibroblasts and monocytes were similar to those results presented by the 2D culture. In general, the cellular absorption and toxicity results are similar between 2D cultures and 3D model, however different results can be obtained due to differences in the penetration of the nanoparticle and in the operating time of the models (Lu and Stenzel, 2018). In according with this concept, different biocompatibility results between 2D culture and double MCTS model were observed. For the double MCTS model, it was verified that the nanoparticles were compatible for all concentrations analyzed, probably due to the morphological limitations of the model, since it is more compact and produce matrix, which can prevent the nanoparticle penetration into to the spheroid, thus being more resistant to treatment compared to the triple model. Furthermore, this compact morphology can also reduce the penetration resazurin to spheroid core and consequently the resazurin is reduced only by a limited number of cells. Importantly, the resazurin assay can generate an unreliable readout to indicate cytotoxicity due to the tight junction state of cells present in spheroids. An intrinsic feature of spheroid formation is the establishment of junctions between the cells (Ivascu and Kubbies, 2007). Similar results were seen by Walzl *et al.*, where they provided convincing evidence that the establishment of tight junctions within or in the surface cell layer of the spheroids prevents resazurin from penetrating the spheroid nucleus (Walzl et al., 2014).

Regarding the ability of Pani/γ-Fe_2O_3 NPs to reprogramming of macrophages in both MCTS models, for the double model, the nanoparticles were not able to exercise any effect on the number of M1 or M2 macrophages, probably due to the morphological features of the model, which can prevent the penetration of nanosystems and reduce their interaction with the particles. For the triple model, we observed that the exposure of Pani/γ-Fe_2O_3 NPs led to increased expression of $CD86^+$ (M1 marker), showing that Pani/γ-Fe_2O_3 NPs can be used as a tool to reprogram macrophage to M1-like phenotype. It is known that iron oxide nanoparticles are powerful carriers for vaccine delivery for cancer treatment (Soetaert et al., 2020; Zhao et al., 2018). They can have a direct effect by polarization of immune cells, such macrophages and DCs, increasing immune response, or can be used as a delivery system, instance of OVA, with a function of immune potentiator (Volovat et al., 2022; Luo et al., 2019).

Various iron oxide nano-based strategies aimed at regulating macrophage polarization have been developed and tested. For example, Zanganeh et al. demonstrated that ferumoxytol, FDA-approved IONPs for iron deficiency treatment, can elicit a transition from M2 to pro-inflammatory M1 phenotypes in solid tumor tissues and suppress tumor growth (Zanganeh et al., 2016). Zhou et al., designed a nanocarrier composed of IONPs and R837 (PLGA-ION-R837@M (PIR@M)) capable of greatly polarizing the TAMs from the M2 phenotype to the M1 antitumor, the polarization is attributed to the fact that Fe_3O_4 NPs mainly activate the IRF5 signaling pathway via iron ions rather than the NF-κB signaling pathway induced by reactive oxygen species (Liu et al., 2020). Mulens-Arias et al., showed that PEI-coated IONPs (PMag) activate macrophages, with increased of IL-12 secretion in culture medium and the regulation of several genes linked to the M1 phenotype. The macrophage activation induced by PMag was partially dependent on

TLR4 (receptor 4) and ROS signaling (Mulens-Arias et al., 2015). It is important to note that the development of studies based on macrophage reprogramming using iron oxide nanoparticles remains largely empirical. Although the mechanism of reprogramming is currently inconclusive, some studies have found that it may be related to intracellular levels of iron in macrophages, production of ROS and pro-inflammatory cytokines (Zanganeh et al., 2016; Wu et al., 2021; Dalzon et al., 2019; Li et al., 2019). The lack of standardization of preclinical studies and the variability of experimental conditions and results still represents a barrier to the creation of therapies based on IONPs (Nascimento et al., 2021).

Our results showed that Pani/γ-Fe_2O_3 NPs have a great potential for macrophage reprogramming and immunotherapy of breast cancer. As they are magnetic and polyaniline-coated, a conducting polymer, they can also be used in photothermal therapy to induce immune responses in tumors and deliver immunostimulants and checkpoint inhibitory molecules to enhance the immune response. Pani/γ-Fe_2O_3 NPs can enhance the effectiveness of other immunotherapies M1-activating against cancer cells such as antibodies, microRNAs and other molecules already known to further amplify the desired immunomodulatory properties (Gordon et al., 2017; Duluc et al., 2009; Wiehagen et al., 2017; Curtale et al., 2019). Finally, Pani/γ-Fe_2O_3 NPs can be used in adoptive cell therapy and T-cell enrichment and as the imaging agents such as magnetic resonance imaging (MRI) contrast and good biodegradability. For Pani/γ-Fe_2O_3 NPs application against tumors, more studies must be conducted to understand its pharmacokinetic, pharmacodynamics, biodistribution and the better administration route to stimulate macrophages, enhancing their activity and response to cancer.

5. Conclusion

IONPs have proved their efficacy in a variety of biomedical applications as drug carriers. An attractive new research area is exploring their ability to activate and reprogram macrophages towards a M1-like profile for application in cancer therapy.

In summary, our work based on polyaniline-coated iron oxide nanoparticles (Pani/γ-Fe_2O_3 NPs) demonstrated that cellular uptake of the nanoparticles by macrophages present in 2D culture and into triple MCTS model causes macrophage reprogramming to the M1-like antitumor phenotype. These properties allow Pani/γ-Fe_2O_3 NPs to alter the orientation of the TME towards an antitumor scenario that may result in the control of breast tumor growth. We believe that this work expands the knowledge about the role of IONPs in the activation of the immune system and contributes to the development of new therapeutic strategies against solid tumors.

In addition, we have also seen that the use of 3D multicellular culture models fills some gaps present in 2D models and improves cancer drug discovery success rates, as they display a microenvironment closer to tumors *in vivo*. Finally, it is concluded that Pani/γ-Fe_2O_3 NPs have the potential to act as a macrophage immunostimulator to M1-phenotype and, consequently, to be able to compose a complementary strategy to the treatment of breast cancer.

CRediT authorship contribution statement

Camila Nascimento: Conceptualization, Methodology, Writing – original draft. **Flávia Castro:** Methodology. **Mariana Domingues:** Methodology. **Anna Lage:** Methodology. **Érica Alves:** Methodology. **Rodrigo de Oliveira:** Methodology. **Celso de Melo:** Methodology. **Carlos Eduardo Calzavara-Silva:** Writing – review & editing. **Bruno Sarmento:** Writing – review & editing, Conceptualization, Supervision.

Declaration of Competing Interest

The authors declare that they have no known competing financial interests or personal relationships that could have appeared to influence the work reported in this paper.

Data availability

Data will be made available on request.

Acknowledgements

This work was financially supported by Coordenadoria de Aperfeiçoamento de Pessoal de Nível Superior (CAPES) and FAPEMIG – Rede Mineira de Nanomedicina Teranóstica (RED-00079-22). The authors thank the René Rachou Institute /FIOCRUZ Minas and flow cytometry platform. This work was also supported by the project Norte-01-0145-FEDER-000051 - "Cancer Research on Therapy Resistance: From Basic Mechanisms to Novel Targets", supported by Norte Portugal Regional Operational Programme (NORTE 2020), under the PORTUGAL 2020 Partnership Agreement, through the European Regional Development Fund (FEDER). The authors also acknowledge the i3S Institute and support of the i3S Scientific Platforms: Advanced Light Microscopy and Translational Cytometry. The authors acknowledge the support of the i3S Scientific Platform HEMS and Ana Rita Malheiro e Rui Fernandes., members of the national infrastructure PPBI - Portuguese Platform of Bioimaging (PPBI-POCI-01-0145-FEDER-022122). F Castro (2021.01773.CEECIND) acknowledge CEEC contract, financed by the Portuguese Science and Technology Foundation (FCT). We also acknowledge Dr. Meriem Lamghari and Sílvia Bidarra, from i3S, Porto, Portugal, for providing the cell lines to this study.

Appendix A. Supplementary data

Supplementary data to this article can be found online at https://doi.org/10.1016/j.ijpharm.2023.122866.

References

Alves, K.G.B., Felix, J.F., De Melo, E.F., Dos Santos, C.G., Andrade, C.A.S., De Melo, C.P., 2012. Characterization of ZnO/polyaniline nanocomposites prepared by using surfactant solutions as polymerization media. J. Appl. Polym. Sci. https://doi.org/10.1002/app.35502.

Biswas, S.K., Mantovani, A., 2010. Macrophage plasticity and interaction with lymphocyte subsets: Cancer as a paradigm. Nat. Immunol. 11, 889–896. https://doi.org/10.1038/ni.1937.

Biswas, S.K., Mantovani, A., 2012. Orchestration of metabolism by macrophages. Cell Metab. 15, 432–437. https://doi.org/10.1016/j.cmet.2011.11.013.

Costa da Silva, M., Breckwoldt, M.O., Vinchi, F., Correia, M.P., Stojanovic, A., Thielmann, C.M., Meister, M., Muley, T., Warth, A., Platten, M., Hentze, M.W., Cerwenka, A., Muckenthaler, M.U., 2017. Iron Induces Anti-tumor Activity in Tumor-Associated Macrophages. Front. Immunol. 8, 1479 https://www.frontiersin.org/article/10.3389/fimmu.2017.01479.

Cronin, S.J.F., Woolf, C.J., Weiss, G., Penninger, J.M., 2019. The Role of Iron Regulation in Immunometabolism and Immune-Related Disease. Front. Mol. Biosci. 6, 116. https://doi.org/10.3389/fmolb.2019.00116.

Curren Smith, E.W., 2015. Macrophage Polarization and Its Role in Cancer. J. Clin Cell. Immunol. 06 https://doi.org/10.4172/2155-9899.1000338.

Curtale, G., Rubino, M., Locati, M., 2019. MicroRNAs as molecular switches in macrophage activation. Front. Immunol. https://doi.org/10.3389/fimmu.2019.00799.

da Silva, R.J., Maciel, B.G., Medina-Llamas, J.C., Chávez-Guajardo, A.E., Alcaraz-Espinoza, J.J., Pinto de Melo, C., 2019. Extraction of plasmid DNA by use of a magnetic maghemite-polyaniline nanocomposite. Anal. Biochem. 575, 27–35. https://doi.org/10.1016/j.ab.2019.03.013.

Dalzon, B., Guidetti, M., Testemale, D., Reymond, S., Proux, O., Vollaire, J., Collin-Faure, V., Testard, I., Fenel, D., Schoehn, G., Arnaud, J., Carrière, M., Josserand, V., Rabilloud, T., Aude-Garcia, C., Yuan, P., Hu, X., Zhou, Q., Laskar, A., Eilertsen, J., Li, W., Yuan, X.M., Chen, S.S., Chen, S.S., Zeng, Y., Lin, L., Wu, C., Ke, Y., Liu, G., Chen, L., Ma, X., Dang, M., Dong, H., Hu, H., Su, X., Liu, W., Wang, Q., Mou, Y., Teng, Z., Mulens-Arias, V., Rojas, J.M., Barber, D.F., Tzetzo, S.L., Abrams, S.I., Mulens-Arias, V., Rojas, J.M., Pérez-Yagüe, S., Morales, M.P., Barber, D.F., Korangath, P., Barnett, J.D., Sharma, A., Henderson, E.T., Stewart, J., Yu, S.H., Kandala, S.K., Yang, C.T., Caserto, J.S., Hedayati, M., Armstrong, T.D., Jaffee, E., Gruettner, C., Zhou, X.C., Fu, W., Hu, C., Sukumar, S., Simons, B.W., Ivkov, R., Gu, Z., Liu, T., Tang, J., Yang, Y., Song, H., Tuong, Z.K., Fu, J., Yu, C., Zanganeh, S., Hutter, G., Spitler, R., Lenkov, O., Mahmoudi, M., Shaw, A., Pajarinen, J.S., Nejadnik, H., Goodman, S., Moseley, M., Coussens, L.M., Daldrup-link, H.E., Xie, Y., Jiang, J., Tang, Q., Zou, H., Zhao, X.X., Liu, H., Ma, D., Cai, C., Zhou, Y., Chen, X.,

Pu, J., Liu, P., Zhang, L.L., Tan, S., Liu, Y., Xie, H., Luo, B.B., Wang, J., Liu, L., Sha, R., Yang, L., Zhao, X.X., Zhu, Y., Gao, J., Zhang, Y., Wen, L.P., Luo, L., Iqbal, M. Z., Liu, C., Xing, J., Akakuru, O.U., Fang, Q., Li, Z., Dai, Y., Li, A., Guan, Y., Wu, A., Zhao, J., Zhang, Z., Xue, Y., Wang, G., Cheng, Y., Pan, Y., Zhao, S., Hou, Y., Jin, R., Liu, L., Zhu, W., Li, D., Yang, L., Duan, J., Cai, Z., Nie, Y., Zhang, Y., Gong, Q., Song, B., Wen, L.P., Anderson, J.M., Ai, H., Li, C.X., Zhang, Y., Dong, X., Zhang, L.L., Liu, M.D., Li, B., Zhang, M.K., Feng, J., Zhang, X.Z., Rojas, J.M., Sanz-Ortega, L., Mulens-Arias, V., Gutiérrez, L., Pérez-Yagüe, S., Barber, D.F., Zhang, W., Cao, S., Liang, S., Tan, C.H., Luo, B.B., Xu, X., Saw, P.E., da Silva, M.C., Breckwoldt, M.O., Vinchi, F., Correia, M.P., Stojanovic, A., Thielmann, C.M., Meister, M., Muley, T., Warth, A., Platten, M., Hentze, M.W., Cerwenka, A., Muckenthaler, M.U., 2019. Impact of Morphology on Iron Oxide Nanoparticles-Induced Inflammasome Activation in Macrophages. Biomaterials 8, 1–10. https://doi.org/10.1177/0885328218817939.

Dukhinova, M.S., Prilepskii, A.Y., Vinogradov, V.V., Shtil, A.A., 2019. Metal oxide nanoparticles in therapeutic regulation of macrophage functions. Nanomaterials 9, 1631. https://doi.org/10.3390/nano9111631.

Duluc, D., Corvaisier, M., Blanchard, S., Catala, L., Descamps, P., Gamelin, E., Ponsoda, S., Delneste, Y., Hebbar, M., Jeannin, P., 2009. Interferon-γ reverses the immunosuppressive and protumoral properties and prevents the generation of human tumor-associated macrophages. Int. J. Cancer 125, 367–373. https://doi.org/10.1002/ijc.24401.

Emens, L.A., 2018. Breast cancer immunotherapy: Facts and hopes. Clin. Cancer Res. 24 https://doi.org/10.1158/1078-0432.CCR-16-3001.

Fritsche, G., Nairz, M., Werner, E.R., Barton, H.C., Weiss, G., 2008. Nramp1-functionality increases iNOS expression via repression of IL-10 formation. Eur. J. Immunol. https://doi.org/10.1002/eji.200838449.

Furgiuele, S., Descamps, G., Cascarano, L., Boucq, A., Dubois, C., Journe, F., Saussez, S., 2022. Dealing with Macrophage Plasticity to Address Therapeutic Challenges in Head and Neck Cancers. Int. J. Mol. Sci. 23 https://doi.org/10.3390/ijms23126385.

Gao, J.J., Swain, S.M., 2018. Luminal A Breast Cancer and Molecular Assays: A Review. Oncologist. https://doi.org/10.1634/theoncologist.2017-0535.

Genard, G., Lucas, S., Michiels, C., 2017. Reprogramming of tumor-associated macrophages with anticancer therapies: Radiotherapy versus chemo- and immunotherapies. Front. Immunol. 14, 828. https://doi.org/10.3389/fimmu.2017.00828.

Gordon, S.R., Maute, R.L., Dulken, B.W., Hutter, G., George, B.M., McCracken, M.N., Gupta, R., Tsai, J.M., Sinha, R., Corey, D., Ring, A.M., Connolly, A.J., Weissman, I.L., 2017. PD-1 expression by tumour-associated macrophages inhibits phagocytosis and tumour immunity. Nature 545, 495–499. https://doi.org/10.1038/nature22396.

Han, S.J., Kwon, S., Kim, K.S., 2021. Challenges of applying multicellular tumor spheroids in preclinical phase. Cancer Cell Int. https://doi.org/10.1186/s12935-021-01853-8.

Itoh, Y., Nagase, H., 2002. Matrix metalloproteinases in cancer. Essays Biochem. https://doi.org/10.1042/bse0380021.

Ivascu, A., Kubbies, M., 2007. Diversity of cell-mediated adhesions in breast cancer spheroids. Int. J. Oncol. 31 https://doi.org/10.3892/ijo.31.6.1403.

Ferlay, J., Ervik, M., Lam, F., Colombet, M., Mery, L., Piñeros, M., Znaor, A., Soerjomataram, I., Bray, F., 2021. Global Cancer Observatory: Cancer Today. Lyon, France: International Agency for Research on Cancer. Available from: https://gco.iarc.fr/today, accessed [29 09 2021], Int. Agency Res. Cancer.

Jeong, S.Y., Lee, J.H., Shin, Y., Chung, S., Kuh, H.J., 2016. Co-culture of tumor spheroids and fibroblasts in a collagen matrix-incorporated microfluidic chip mimics reciprocal activation in solid tumor microenvironment. PLoS One. https://doi.org/10.1371/journal.pone.0159013.

Jung, M., Mertens, C., Brüne, B., 2015. Macrophage iron homeostasis and polarization in the context of cancer. Immunobiology 220, 295–304. https://doi.org/10.1016/j.imbio.2014.09.011.

Jung, M., Weigert, A., Mertens, C., Rehwald, C., Brüne, B., 2017. Iron handling in tumor-associated macrophages-Is there a new role for lipocalin-2? Front. Immunol. 8, 1171. https://doi.org/10.3389/fimmu.2017.01171.

Jung, M., Mertens, C., Tomat, E., Brüne, B., 2019. Iron as a central player and promising target in cancer progression. Int. J. Mol. Sci. 20, 273. https://doi.org/10.3390/ijms20020273.

Kao, J.K., Wang, S.C., Ho, L.W., Huang, S.W., Lee, C.H., Lee, M.S., Yang, R.C., Shieh, J.J., 2020. M2-like polarization of THP-1 monocyte-derived macrophages under chronic iron overload. Ann. Hematol. 99, 431–441. https://doi.org/10.1007/s00277-020-03916-8.

Khan, A., Aldwayyan, A.S., Alhoshan, M., Alsalhi, M., 2010. Synthesis by in situ chemical oxidative polymerization and characterization of polyaniline/iron oxide nanoparticle composite. Polym. Int. 59, 1690–1694. https://doi.org/10.1002/pi.2908.

Kuen, J., Darowski, D., Kluge, T., Majety, M., 2017. Pancreatic cancer cell/fibroblast co-culture induces M2 like macrophages that influence therapeutic response in a 3D model. PLoS One. https://doi.org/10.1371/journal.pone.0182039.

Laskar, A., Eilertsen, J., Li, W., Yuan, X.M., 2013. SPION primes THP1 derived M2 macrophages towards M1-like macrophages. Biochem. Biophys. Res. Commun. 441, 737–742. https://doi.org/10.1016/j.bbrc.2013.10.115.

Lazzari, G., Couvreur, P., Mura, S., 2017. Multicellular tumor spheroids: A relevant 3D model for the: In vitro preclinical investigation of polymer nanomedicines. Polym. Chem. 8 https://doi.org/10.1039/c7py00559h.

Lee Ventola, C., 2017. Cancer immunotherapy, part 1: Current strategies and agents. P T. 42, 375–383.

Lei, P., Bai, T., Sun, Y., 2019. Mechanisms of ferroptosis and relations with regulated cell death: A review. Front. Physiol. https://doi.org/10.3389/fphys.2019.00139.

Li, C.X., Zhang, Y., Dong, X., Zhang, L., Liu, M.D., Li, B., Zhang, M.K., Feng, J., Zhang, X. Z., 2019. Artificially Reprogrammed Macrophages as Tumor-Tropic Immunosuppression-Resistant Biologics to Realize Therapeutics Production and Immune Activation. Adv. Mater. 31, 1807211. https://doi.org/10.1002/adma.201807211.

Li, C.X., Zhang, Y., Dong, X., Zhang, L., Liu, M.D., Li, B., Zhang, M.K., Feng, J., Zhang, X. Z., 2019. Artificially Reprogrammed Macrophages as Tumor-Tropic Immunosuppression-Resistant Biologics to Realize Therapeutics Production and Immune Activation. Adv. Mater. https://doi.org/10.1002/adma.201807211.

Li, C.X., Zhang, Y., Dong, X., Zhang, L., Liu, M.D., Li, B., Zhang, M.K., Feng, J., Zhang, X. Z., 2019. Artificially Reprogrammed Macrophages as Tumor-Tropic Immunosuppression-Resistant Biologics to Realize Therapeutics Production and Immune Activation. Adv. Mater. 31, 1–11. https://doi.org/10.1002/adma.201807211.

Linde, N., Casanova-Acebes, M., Sosa, M.S., Mortha, A., Rahman, A., Farias, E., Harper, K., Tardio, E., Reyes Torres, I., Jones, J., Condeelis, J., Merad, M., Aguirre-Ghiso, J.A., 2018. Macrophages orchestrate breast cancer early dissemination and metastasis. Nat. Commun. 9 https://doi.org/10.1038/s41467-017-02481-5.

Liu, L., Wang, Y., Guo, X., Zhao, J., Zhou, S., 2020. A Biomimetic Polymer Magnetic Nanocarrier Polarizing Tumor-Associated Macrophages for Potentiating Immunotherapy. Small 16. https://doi.org/10.1002/smll.202003543.

Lu, H., Stenzel, M.H., 2018. Multicellular Tumor Spheroids (MCTS) as a 3D In Vitro Evaluation Tool of Nanoparticles. Small. https://doi.org/10.1002/smll.201702858.

Lukianova-Hleb, E.Y., Kim, Y.S., Belatsarkouski, I., Gillenwater, A.M., O'Neill, B.E., Lapotko, D.O., 2016. Intraoperative diagnostics and elimination of residual microtumours with plasmonic nanobubbles. Nat. Nanotechnol. 11, 525–532. https://doi.org/10.1038/nnano.2015.343.

Luo, L., Iqbal, M.Z., Liu, C., Xing, J., Akakuru, O.U., Fang, Q., Li, Z., Dai, Y., Li, A., Guan, Y., Wu, A., 2019. Engineered nano-immunopotentiators efficiently promote cancer immunotherapy for inhibiting and preventing lung metastasis of melanoma. Biomaterials 223. https://doi.org/10.1016/j.biomaterials.2019.119464.

Madsen, N.H., Nielsen, B.S., Nhat, S.L., Skov, S., Gad, M., Larsen, J., 2021. Monocyte infiltration and differentiation in 3d multicellular spheroid cancer models. Pathogens. https://doi.org/10.3390/pathogens10080969.

Mantovani, A., Sica, A., Sozzani, S., Allavena, P., Vecchi, A., Locati, M., 2004. The chemokine system in diverse forms of macrophage activation and polarization. Trends Immunol. https://doi.org/10.1016/j.it.2004.09.015.

Mantovani, A., Marchesi, F., Malesci, A., Laghi, L., Allavena, P., 2017. Tumour-associated macrophages as treatment targets in oncology. Nat. Rev. Clin. Oncol. 14, 399–416. https://doi.org/10.1038/nrclinonc.2016.217.

McCawley, L.J., Matrisian, L.M., 2001. Matrix metalloproteinases: They're not just for matrix anymore! Curr. Opin. Cell Biol. https://doi.org/10.1016/S0955-0674(00)00248-9.

Mulens-Arias, V., Rojas, J.M., Pérez-Yagüe, S., Morales, M.P., Barber, D.F., 2015. Polyethylenimine-coated SPIONs trigger macrophage activation through TLR-4 signaling and ROS production and modulate podosome dynamics. Biomaterials. https://doi.org/10.1016/j.biomaterials.2015.02.068.

Mulero, V., Searle, S., Blackwell, J.M., Brock, J.H., 2002. Solute carrier 11a1 (Slc11a1; formerly Nramp1) regulates metabolism and release of iron acquired by phagocytic, but not transferrin-receptor-mediated, iron uptake. Biochem. J. https://doi.org/10.1042/0264-6021:3630089.

Murray, P.J., 2017. Macrophage Polarization. Annu. Rev. Physiol. 79, 541–566. https://doi.org/10.1146/annurev-physiol-022516-034339.

Nascimento, C.S., Alves, É.A.R., de Melo, C.P., Corrêa-Oliveira, R., Calzavara-Silva, C.E., 2021. Immunotherapy for cancer: effects of iron oxide nanoparticles on polarization of tumor-associated macrophages. Nanomedicine (Lond) 16, 2633–2650. https://doi.org/10.2217/nnm-2021-0255.

Okazaki, Y., Chew, S.H., Nagai, H., Yamashita, Y., Ohara, H., Jiang, L., Akatsuka, S., Takahashi, T., Toyokuni, S., 2020. Overexpression of miR-199/214 is a distinctive feature of iron-induced and asbestos-induced sarcomatoid mesothelioma in rats. Cancer Sci. 111, 2016–2027. https://doi.org/10.1111/cas.14405.

Rahimi, A.A.R., Gee, K., Mishra, S., Lim, W., Kumar, A., 2005. STAT-1 Mediates the Stimulatory Effect of IL-10 on CD14 Expression in Human Monocytic Cells. J. Immunol. https://doi.org/10.4049/jimmunol.174.12.7823.

Rajendran, A., 2017. Synthesis, Characterization and Electrical Properties of Nano Metal and Metal-Oxide Doped with Conducting Polymer Composites by in-Situ Chemical Polymerization. MOJ Polym. Sci. 1, 2–6. https://doi.org/10.15406/mojps.2017.01.00031.

Recalcati, S., Cairo, G., 2021. Macrophages and iron: A special relationship. Biomedicines. https://doi.org/10.3390/biomedicines9111585.

Recalcati, S., Locati, M., Marini, A., Santambrogio, P., Zaninotto, F., De Pizzol, M., Zammataro, L., Girelli, D., Cairo, G., 2010. Differential regulation of iron homeostasis during human macrophage polarized activation. Eur. J. Immunol. 40, 824–835. https://doi.org/10.1002/eji.200939889.

Recalcati, S., Gammella, E., Cairo, G., 2019. Ironing out macrophage immunometabolism. Pharmaceuticals. 12, 94–104. https://doi.org/10.3390/ph12020094.

Sacco, A., Battaglia, A.M., Botta, C., Aversa, I., Mancuso, S., Costanzo, F., Biamonte, F., 2021. Iron metabolism in the tumor microenvironment— implications for anti-cancer immune response. Cells. 10 https://doi.org/10.3390/cells10020303.

Sandanger, Ø., Ryan, L., Bohnhorst, J., Iversen, A.-C., Husebye, H., Halaas, Ø., Landrø, L., Aukrust, P., Frøland, S.S., Elson, G., Visintin, A., Øktedalen, O., Damås, J.K., Sundan, A., Golenbock, D., Espevik, T., 2009. IL-10 Enhances MD-2 and CD14 Expression in Monocytes and the Proteins Are Increased and Correlated in HIV-Infected Patients. J. Immunol. https://doi.org/10.4049/jimmunol.182.1.588.

Silverstein, K., 2005. Webster, Spectrometric Identification of Organic Compounds 7th Edition.
Sim, B., Chae, H.S., Choi, H.J., 2015. Fabrication of polyaniline coated iron oxide hybrid particles and their dual stimuli-response under electric and magnetic fields. Express Polym. Lett. 9, 736–743. https://doi.org/10.3144/expresspolymlett.2015.68.
Sirén, V., Salmenperä, P., Kankuri, E., Bizik, J., Sorsa, T., Tervahartiala, T., Vaheri, A., 2006. Cell-cell contact activation of fibroblasts increases the expression of matrix metalloproteinases. Ann. Med. https://doi.org/10.1080/07853890500494999.
Soetaert, F., Korangath, P., Serantes, D., Fiering, S., Ivkov, R., 2020. Cancer therapy with iron oxide nanoparticles: Agents of thermal and immune therapies. Adv. Drug Deliv. Rev. https://doi.org/10.1016/j.addr.2020.06.025.
Sydulu Singu, B., Srinivasan, P., Pabba, S., 2011. Benzoyl Peroxide Oxidation Route to Nano Form Polyaniline Salt Containing Dual Dopants for Pseudocapacitor. J. Electrochem. Soc. 159, A6–A13. https://doi.org/10.1149/2.036201jes.
Vinchi, F., 2018. Shaping macrophage plasticity with iron - Towards a new therapeutic approach, Eur. Oncol. Haematol. 10.17925/EOH.2018.14.2.76.
Vinogradov, S., Wei, X., 2012. Cancer stem cells and drug resistance: The potential of nanomedicine. Nanomedicine. https://doi.org/10.2217/nnm.12.22.
Volovat, C., Volovat, S.R., Agop, M., 2022. Nanotechnology and Immunomodulators in Cancer BT - Immunomodulators and Human Health. In: Kesharwani, R.K., Keservani, R.K., Sharma, A.K. (Eds.), Springer Nature Singapore, Singapore, pp. 125–186. 10.1007/978-981-16-6379-6_5.
Walzl, A., Unger, C., Kramer, N., Unterleuthner, D., Scherzer, M., Hengstschläger, M., Schwanzer-Pfeiffer, D., Dolznig, H., 2014. The resazurin reduction assay can distinguish cytotoxic from cytostatic compounds in spheroid screening assays. J. Biomol. Screen. 19, 1047–1059. https://doi.org/10.1177/1087057114532352.
Wiehagen, K.R., Girgis, N.M., Yamada, D.H., Smith, A.A., Chan, S.R., Grewal, I.S., Quigley, M., Verona, R.I., 2017. Combination of CD40 agonism and CSF-1R blockade reconditions tumor-associated macrophages and drives potent antitumor immunity. Cancer Immunol. Res. 5, 1109–1121. https://doi.org/10.1158/2326-6066.CIR-17-0258.
Wild, C., Weiderpass, E., Stewart, B., 2020. World Cancer Report: Cancer Research for Cancer Prevention, Lyon, France: International Agency for Research on Cancer. http://publications.iarc.fr/586.
Wu, X., Cheng, Y., Zheng, R., Xu, K., Yan, J., Song, P., Wang, Y., Rauf, A., Pan, Y., Zhang, H., 2021. Immunomodulation of Tumor Microenvironment by Arginine-Loaded Iron Oxide Nanoparticles for Gaseous Immunotherapy. ACS Appl. Mater. Interfaces 13, 19825–19835. https://doi.org/10.1021/acsami.1c04638.
Wu, W., He, Q., Jiang, C., 2008. Magnetic iron oxide nanoparticles: Synthesis and surface functionalization strategies. Nanoscale Res. Lett. https://doi.org/10.1007/s11671-008-9174-9.
Zanganeh, S., Hutter, G., Spitler, R., Lenkov, O., Mahmoudi, M., Shaw, A., Pajarinen, J.S., Nejadnik, H., Goodman, S., Moseley, M., Coussens, L.M., Daldrup-Link, H.E., 2016. Iron oxide nanoparticles inhibit tumour growth by inducing pro-inflammatory macrophage polarization in tumour tissues. Nat. Nanotechnol. 11, 986–994. https://doi.org/10.1038/nnano.2016.168.
Zanoni, M., Piccinini, F., Arienti, C., Zamagni, A., Santi, S., Polico, R., Bevilacqua, A., Tesei, A., 2016. 3D tumor spheroid models for in vitro therapeutic screening: A systematic approach to enhance the biological relevance of data obtained. Sci. Rep. https://doi.org/10.1038/srep19103.
Zhang, W., Cao, S., Liang, S., Tan, C.H., Luo, B., Xu, X., Saw, P.E., 2020. Differently Charged Super-Paramagnetic Iron Oxide Nanoparticles Preferentially Induced M1-Like Phenotype of Macrophages. Front. Bioeng. Biotechnol. 8, 537 https://www.frontiersin.org/article/10.3389/fbioe.2020.00537.
Zhao, J., Zhang, Z., Xue, Y., Wang, G., Cheng, Y., Pan, Y., Zhao, S., Hou, Y., 2018. Anti-tumor macrophages activated by ferumoxytol combined or surface-functionalized with the TLR3 agonist poly (I: C) promote melanoma regression. Theranostics. 8, 6307–6321. https://doi.org/10.7150/thno.29746.
Zhao, Y., Zhao, X., Cheng, Y., Guo, X., Yuan, W., 2018. Iron Oxide Nanoparticles-Based Vaccine Delivery for Cancer Treatment. Mol. Pharm. 15, 1791–1799. https://doi.org/10.1021/acs.molpharmaceut.7b01103.
Zhou, Y., Que, K.T., Tang, H.M., Zhang, P., Fu, Q.M., Liu, Z.J., 2020. Anti-CD206 antibody-conjugated Fe3O4-based PLGA nanoparticles selectively promote tumor-associated macrophages to polarize to the pro-inflammatory subtype. Oncol. Lett. 20, 298. https://doi.org/10.3892/OL.2020.12161.
Zhu, L., Zhao, Q., Yang, T., Ding, W., Zhao, Y., 2015. Cellular metabolism and macrophage functional polarization. Int. Rev. Immunol. https://doi.org/10.3109/08830185.2014.969421.